Clays and Clay Minerals, Vol. 63, No. 4, 235–261, 2015.

SEDIMENT-HOSTED KAOLIN DEPOSIT FROM ÇAKMAKTEPE (UŞAK, TURKEY): ITS MINERALOGY, GEOCHEMISTRY, AND GENESIS

A. YILDIZ AND C. BAŞARAN*

Afyon Kocatepe University, Engineering Faculty, Department of Geological Engineering, Afyonkarahisar, Turkey

Abstract—Because of their geochemical properties, the Çakmaktepe (Uşak) kaolin deposits have been considered as primary. New sedimentological, mineralogical, and geochemical data suggest that the Çakmaktepe kaolins are secondary deposits of sedimentary processes after hydrothermal alteration of the source rocks. The kaolins in the Çakmaktepe deposit were formed from the hydrothermal alteration of calc-alkaline Karaboldere volcanics (KBV). The kaolinized materials were then reworked and accumulated in a lacustrine basin. The argillic alteration zones were associated with faults, and lateral zonation of minerals was observed in the KBV. Smectite was the major phyllosilicate in the 'outer zone'. The alteration mineralogy of the 'inner zone' was similar to that of the Çakmaktepe kaolins and consisted mainly of kaolinite with minor amounts of smectite and alunite. The trace-element abundances in the kaolinized volcanics and the Çakmaktepe kaolins indicated hypogene conditions. The $\delta^{18}O$ values of the Çakmaktepe kaolins ranged from 0.2 to 5.92‰, which indicated that the Çakmaktepe kaolinites were formed at temperatures between 92 and 156ºC, and the δD values ranged from −91.68 to −109.45‰. The irregular edge-to-face morphology, the variation in grain-size, a few broken crystals of kaolinite, the deficiency of dissolution-replacement and crystallization mechanisms, and the the low sphericity, very angular, and poorly sorted quartz crystals in the kaolins all result from transport processes. The sedimentary structures, including trough cross-lamination, tool marks, and load casts, indicate transportation by turbulent waters and deposition of kaolin layers in a shallow lake.

Key Words—Genesis, Kaolin, Mineralogy, O and H Stable Isotopes, Turkey, Uşak.

INTRODUCTION

Kaolins are clays composed mainly of kaolinite minerals. Kaolin deposits are classified as primary and secondary. Primary kaolins include hydrothermal and residual kaolins, and secondary kaolins include sedimentary deposits (Bristow, 1987; Murray, 1988; Murray and Keller, 1993). The primary kaolins are derived from the *in situ* alteration of crystalline rocks, such as granites, rhyolites, andesitic tuffs, and arkosic sandstones. Alterations in primary kaolins may also originate from surface weathering (Supergene Type), hydrothermal activity (Hypogene Type), or a combination of the two. Secondary kaolins are consequences of sedimentary processes and are altered, transported, and deposited as beds or lenses in lacustrine or lagoonal environments. Some primary kaolins are indicators of precious-metal deposits (Hedenquist *et al*., 2000; Dominquez *et al.*, 2010), and secondary kaolins generally have greater economic value than primary kaolin due to their low alunite and Fe-Ti oxide contents (Murray, 1980, 2000; Ekosse, 2000).

The production of kaolin in Turkey increased by 7% in 2011 to ~775,000 metric tons (TUIK, 2014). The most important kaolin deposits in Turkey are located in western Anatolia. Balıkesir-Sındırgı-Düvertepe, Çanakkale-Sarıbeyli-Sığırlı-Bodurlu and Çanakkale-Çan-Çaltıkara-Bahadırlı, Bursa-Mustafa Kemalpaşa, Kütahya-Emet-Hisarcık-Yüylük-Akçakalan-Yağmurlar, Bilecik-Söğüt, and Uşak-Karaçayır are the main primary kaolin-producing provinces in western Anatolia. Most of these kaolins are are derived from the hydrothermal alteration of volcanic rocks (Seyhan, 1978; Çelik *et al.*, 1999; Karakaya *et al.*, 2001; Ece and Schroeder, 2007; Ece *et al.*, 2008; Kadir and Kart, 2009; Karakaya, 2009; Kadir *et al.*, 2011; Kadir and Erkoyun, 2012; Ece *et al.*, 2013). The kaolins in İstanbul-Şile are secondary deposits that were formed by hydrothermal alteration, weathering, transportation, and deposition processes (Ece *et al.*, 2003). The types and amounts of impurities, such as alunite and Fe-Ti oxides, affect adversely the quality of kaolin (Prasad *et al.*, 1991). The greatest problem in Turkish kaolin is kaolins left unprocessed due to such contamination (DPT, 2001).

Numerous studies have been conducted in the study area regarding the distribution and mapping of active fault zones, the hydrogeochemical and geophysical properties of geothermal waters, and the geology, mineralogy, and geochemistry of boron and kaolin deposits (Helvacı, 1986; Taşdelen, 1987; Fujii *et al.*, 1995; Aydoğan *et al.*, 2006; Sayın, 2007; Koçyiğit and Deveci, 2007; Davraz, 2008). Hydrothermal kaolin deposits in Uşak-Karaçayır, Kütahya-Simav-Hisarcık-Yüylük-Gediz, and Balıkesir-Düvertepe-Turplu are located in the same region and have similar geological properties to those of the Çakmaktepe deposit regarding

* E-mail address of corresponding author:
cbasaran@aku.edu.tr
DOI: 10.1346/CCMN.2015.0630401

their country rocks, tectonic evolution, and volcanism (Kadir *et al.*, 2011; Kadir and Erkoyun, 2012; Ece *et al.*, 2013). The Çakmaktepe kaolin deposit is located 50 km southeast of Uşak (western Turkey) and has been exploited for ceramic purposes. The genesis of the Çakmaktepe kaolin deposit has been debated. The genesis of the kaolin deposit was linked by Fujii *et al.* (1995) to sedimentary processes, but kaolinization was stated by Erkoyun and Kadir (2011) to have occurred as a result of acidic hydrothermal fluids and controlled by tectonic activity. The aims of the present study were to resolve the controversy regarding the genesis of the Çakmaktepe kaolin deposit and to contribute to discussions on geology, mineralogy, geochemistry and the

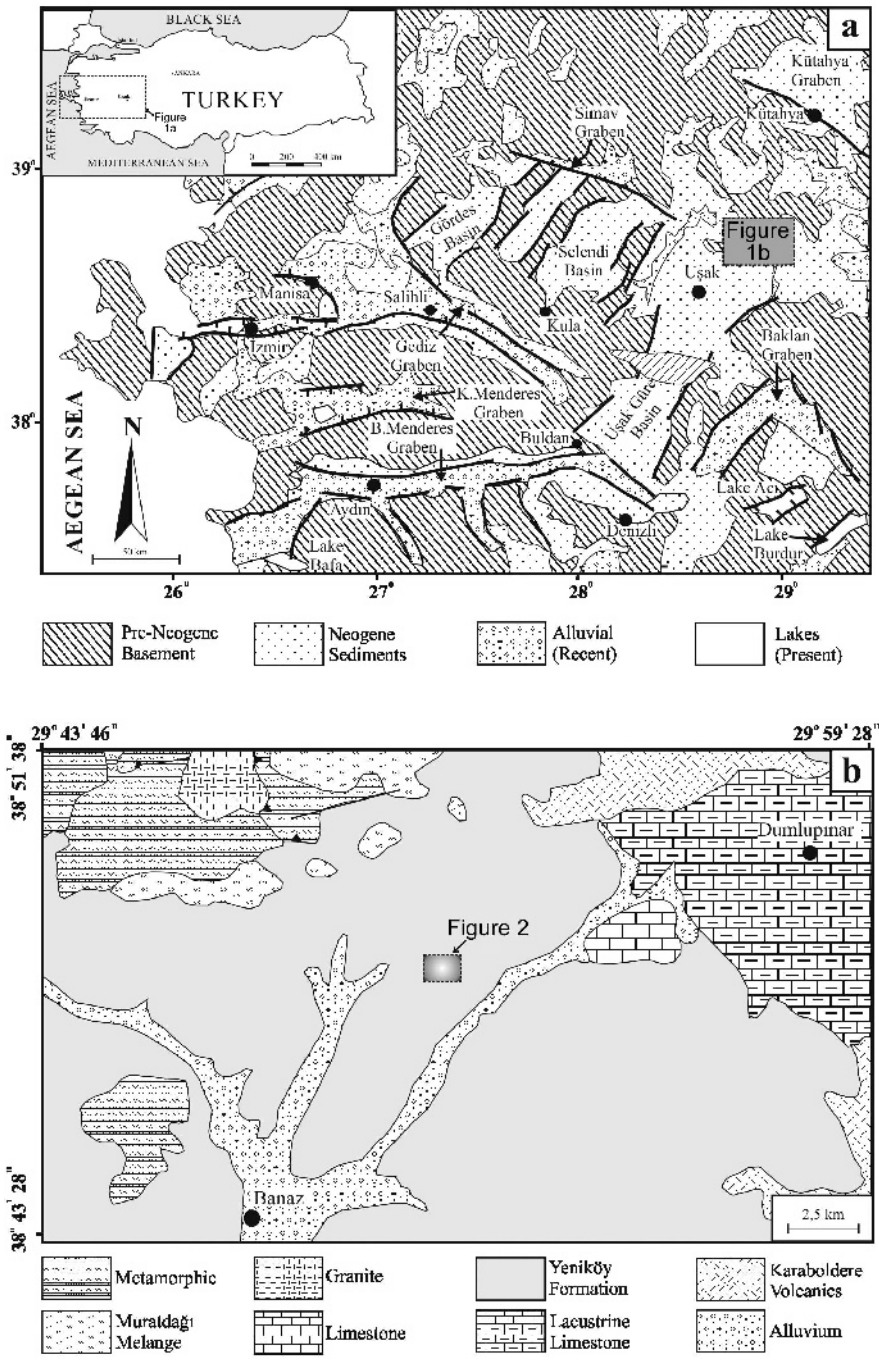

Figure 1. (a) Outline geological map of southwestern Turkey (from Bozkurt and Mittwede, 2002, reproduced with permission), and (b) simplified geological map of Banaz (Uşak) and the surrounding area (from Konak, 2002, reproduced with permission).

https://doi.org/10.1346/CCMN.2015.0630401 Published online by Cambridge University Press

origin of kaolin deposits in western Anatolia and around the world. The kaolin mine in the Çakmaktepe district provides an excellent opportunity for geological study because the mature production faces allowed detailed studies and sampling of clay sedimentology. In the present work, the lithological characteristics of the kaolin deposit were elucidated to explain its transportation and sedimentation conditions. The mineralogical and chemical results from various stratigraphic intervals of the Çakmaktepe deposit and the alteration zones of volcanic rocks in the study area were used to determine the genesis of the deposit. Our results suggest the presence of new kaolin deposits with similar geological properties in western Anatolia that will provide kaolins with small alunite and Fe-Ti oxide contents to the ceramic, paper, rubber, paint, plastic, and pharmaceutical industries in Turkey.

GEOLOGICAL SETTING

Western Turkey has experienced N–S-oriented continental extension since the latest Oligocene–Early Miocene (Bozkurt and Mittwede, 2005). Graben and associated normal fault systems are therefore the dominant structural elements in this region (Figure 1a) (Yılmaz *et al.*, 2000; Koçyiğit and Deveci, 2007; Bozkurt Çiftci and Bozkurt, 2009). The basement rocks in the study area are Paleozoic metasedimentary rocks in the Menderes Massif and the Cretaceous Muratdağı Mélange (Figure 1b), and Lower–Middle Miocene granite intrudes the metamorphic and ultramafic rocks (Aydoğan *et al.*, 2006). The Yeniköy formation unconformably overlies the basement rocks and consists of conglomerate, sandstone, siltstone, marl, and limestone. Based on paleontological data, Ercan *et al.* (1978) demonstrated that these rocks were deposited in fluvial and lacustrine environments and that the Yeniköy formation formed during the Middle–Late Miocene. The Karaboldere volcanics (KBV) showed lateral and vertical gradations with the sedimentary rocks of the Yeniköy formation (Figure 1b).

According to Ercan *et al.* (1979, 1996), Yılmaz *et al.* (2001), Başaran (2009), and Karaoğlu *et al.* (2010), the volcanic rocks around Uşak and the surrounding area were formed during the Early–Middle Miocene due to the collision of the African plate with the Eurasian plate. The KBV formed from trachyandesitic lavas and pyroclastics (*e.g.* agglomerates) in a subduction-related tectonic setting and are calc-alkaline (Başaran, 2009). These volcanites were spheroidally weathered, and are considered to be the source of the Çakmaktepe kaolins. The volcanites have been subjected to NE–SW-oriented normal faults in the Sivaslı-Banaz fault zone (Koçyiğit and Deveci, 2007). Fault-related argillic alterations were observed in the KBV outcrops in the Kozören district 5 km from the Çakmaktepe region (Figure 2). Elongation of the alteration zones was conformable with the orientation of the normal faults (strike N60E

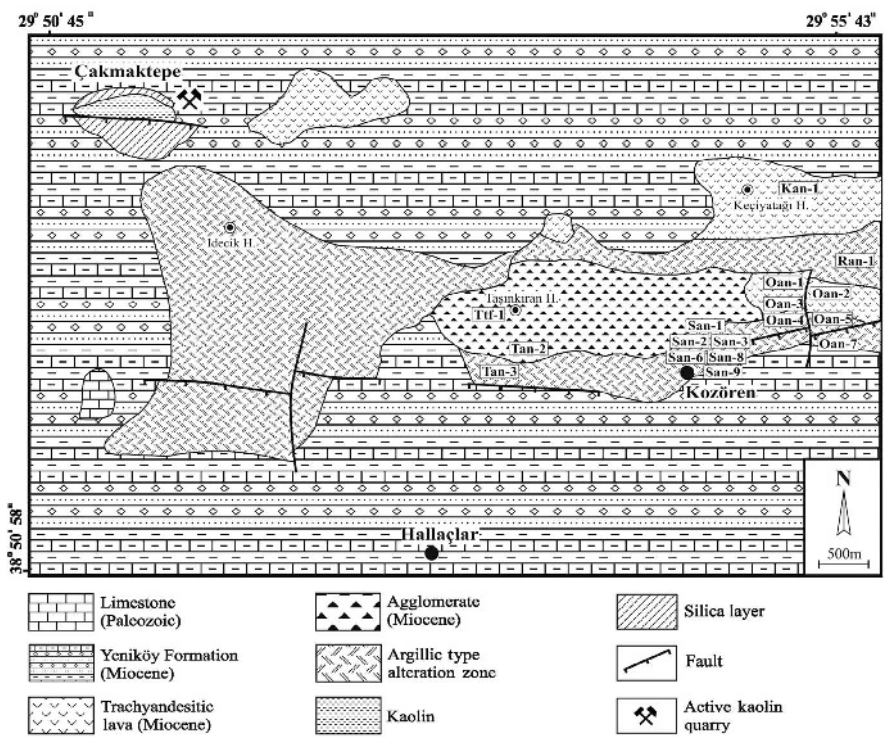

Figure 2. Detailed geological map of Çakmaktepe region.

https://doi.org/10.1346/CCMN.2015.0630401 Published online by Cambridge University Press

and dip 80SE). Three alteration zones were recognized in the KBV. In the outer parts of the alteration, smectite-rich zones (Zone-1) were formed from the alteration of the glassy matrix of the host rock (Oan-7 and San-6). In the inner parts, a glassy matrix and feldspar phenocrysts were altered to form kaolinites (Zone-2: Oan-3, Oan-4, and San-3). In the kaolinitic zone, smaller abundances of smectite minerals were associated with the kaolinites. Fe-oxide and gypsum zones (Zone-3: San-9) nearly 20−30 cm thick and which were consistent in orientations with the fault planes observed in the kaolinite-rich area.

ANALYTICAL METHODS

Twenty four samples were collected from the wall of a kaolin mine in the Çakmaktepe district (Figure 2). Seventeen fresh/unaltered and altered volcanic rock samples were also obtained from the argillic alteration zones of the KBV. The locations of these samples are shown in a detailed geological map of the Çakmaktepe region (Figure 2).

The clay mineralogy was determined by studying <2 μm particles. After dispersing the samples in distilled water overnight, the <2 μm size fraction was separated by sedimentation and subsequent centrifugation. Oriented samples were prepared from the clay fraction spread on glass slides and allowed to dry under atmospheric conditions. The dried samples were saturated with ethylene-glycol vapor at 60ºC and heated at 550ºC for 2 h. The X-ray diffraction (XRD) analyses of the oriented samples were performed on air-dried, ethylene glycol-solvated, and heated samples (Brown, 1972; Brown and Brindley, 1980; MacEwan and Wilson, 1980) to identify the mineral abundances in the kaolins, the kaolinite-bearing samples (KBS), and the altered volcanic rocks, and to determine the degree of structural disorder in the kaolinites. To differentiate halloysite from kaolinite, a formamide test was applied to the clay-sized samples before XRD analysis (Churchman *et al.*, 1984). Bulk samples as random powders and the oriented <2 μm fractions were examined using a Shimadzu XRD-6000 diffractometer (computerized control unit operating at 40 kV and 30 mA using Ni-filtered CuKα radiation). The scanned range was 2−70º2θ in bulk samples and 2−30º2θ in oriented samples at a scanning speed of 2º2θ/min for all samples.

The mineral abundances of the samples were determined using a standardless semi-quantitative analysis, as described by Chung (1974). The Hinckley crystallinity indices of kaolinite were measured on un-oriented XRD patterns from powder samples of the clay fraction.

Freshly broken samples were attached using carbon adhesive on an aluminum substrate, coated with carbon, and surfaces examined using a JEOL-6400 Scanning Electron Microscope with an energy-dispersive X-ray spectrometer (SEM-EDX, Röntec Xflash Detector Type 1105) for morphological studies and microchemical analyses.

Major- and trace-element analyses, including the rare earth element (*REE*) abundances, of the volcanic rocks, bulk kaolins, and KBS were performed in the ACME analytical laboratory in Canada. The total abundances of the major oxides and several minor elements were reported for a 0.1 g sample that was analyzed using inductively coupled plasma-optical emission spectrometry (ICP-OES, Arcos-Spectro, Germany) following lithium metaborate/tetraborate fusion and dilute nitric acid digestion. The loss on ignition (LOI) was measured after heating to 1000ºC. The trace and rare earth element concentrations were determined using inductively coupled plasma-mass spectrometry (ICP-MS, Elan-Perkin Elmer, USA) following lithium metaborate/tetraborate fusion and nitric acid digestion of a 0.1 g sample. The detection limits for the analyses were between 0.01 and 0.1 wt.% for the major elements, 0.1−5 ppm for the trace elements, and 0.01−0.5 ppm for the *REE*.

The major and trace-element abundances of the altered volcanics were normalized with respect to the fresh volcanic rocks to identify elemental behaviors during alteration. Zr was considered to be an immobile element in these calculations based on its relative correlation coefficients with other elements. The mass changes were calculated from the following relationships described by MacLean and Kranidiotis (1987) by using an average starting mass of 100 g of fresh volcanic rock due to the low density differences between the fresh (2.54 g/cm^3) and altered volcanics (2.37 g/cm^3 for the smectitic zone, 2.32 g/cm^3 for the kaolinitic zone). The following equation for (ΔC) applies to SiO_2:

$$\Delta C\ (SiO_2) = \frac{SiO_2\ \text{wt.\% of altered rock}}{\text{Zr ppm of altered rock}} \times \text{Zr ppm of fresh rock}$$

The losses and gains of all the major elements, trace elements, and *REE*s (RC) were computed as the differences between the (ΔC) values of the altered and fresh samples. The $(La/Yb)_{cn}$, (cn: Chondrite normalized) $(La/Sm)_{cn}$, $(Gd/Yb)_{cn}$, and $(Eu/Eu^*)_{cn}$ parameters were normalized according to Sun and McDonough (1989). The $(Ce/Ce^*)_{cn}$ ratio was calculated as $Ce_{cn}/(La_{cn} \times Pr_{cn})^{1/2}$ (McDonough and Sun, 1995).

Oxygen- and hydrogen-isotope analyses were performed on seven pure kaolin samples (Kao-2, Kao-4, Kao-5, Kao-6, Kas-1, Kas-3, and Slt-2) obtained from the <2 μm fractions. The oxygen-isotope analysis was conducted using a Thermo Delta V isotope ratio mass spectrometer (IRMS) interfaced with a Temperature Conversion Elemental Analyzer (TC/EA) in the isotope laboratory at Cornell University (USA). The samples were pyrolyzed at 1375ºC and converted to CO gas. The CO was analyzed against several internal and international standards, and the $^{18}O/^{16}O$ ratios were measured. Hydrogen isotope analysis was also performed by way of pyrolysis using the TC/EA interfaced with the Delta V

https://doi.org/10.1346/CCMN.2015.0630401 Published online by Cambridge University Press

IRMS. Both of the isotopic ratios were analyzed from the same sample matrix in dual analysis mode. The isotopic ratios of oxygen and hydrogen are presented as the permil deviation with respect to the Vienna Standard Mean Ocean Water (VSMOW) standard. The results were reproducible with standard deviations (δD) of >3‰ for hydrogen and 0.4‰ for oxygen.

RESULTS

The lithology of the kaolin deposit

Clastic sedimentary rocks in the Yeniköy formation, such as sandstone and siltstone, host the deposit, which displayed nearly horizontal stratification. The extension of the ESE–WNW-trending normal faults associated with the fault system of western Turkey controlled the distribution of the kaolin deposit (Figure 2). The lithology of the kaolin intervals was laterally uniform. The classifications of Dunham (1962) and Nichols (2009a) for carbonate and clastic sediments, respectively, were applied to identify the sedimentary rocks in the study area (Figure 3).

The deposit consisted primarily of poorly sorted terrigenous clastic sediments, kaolins, and carbonate rocks. In the stratigraphic profile of the deposit, the layers of siltstone (SLST), kaolin (KAO), sand bed

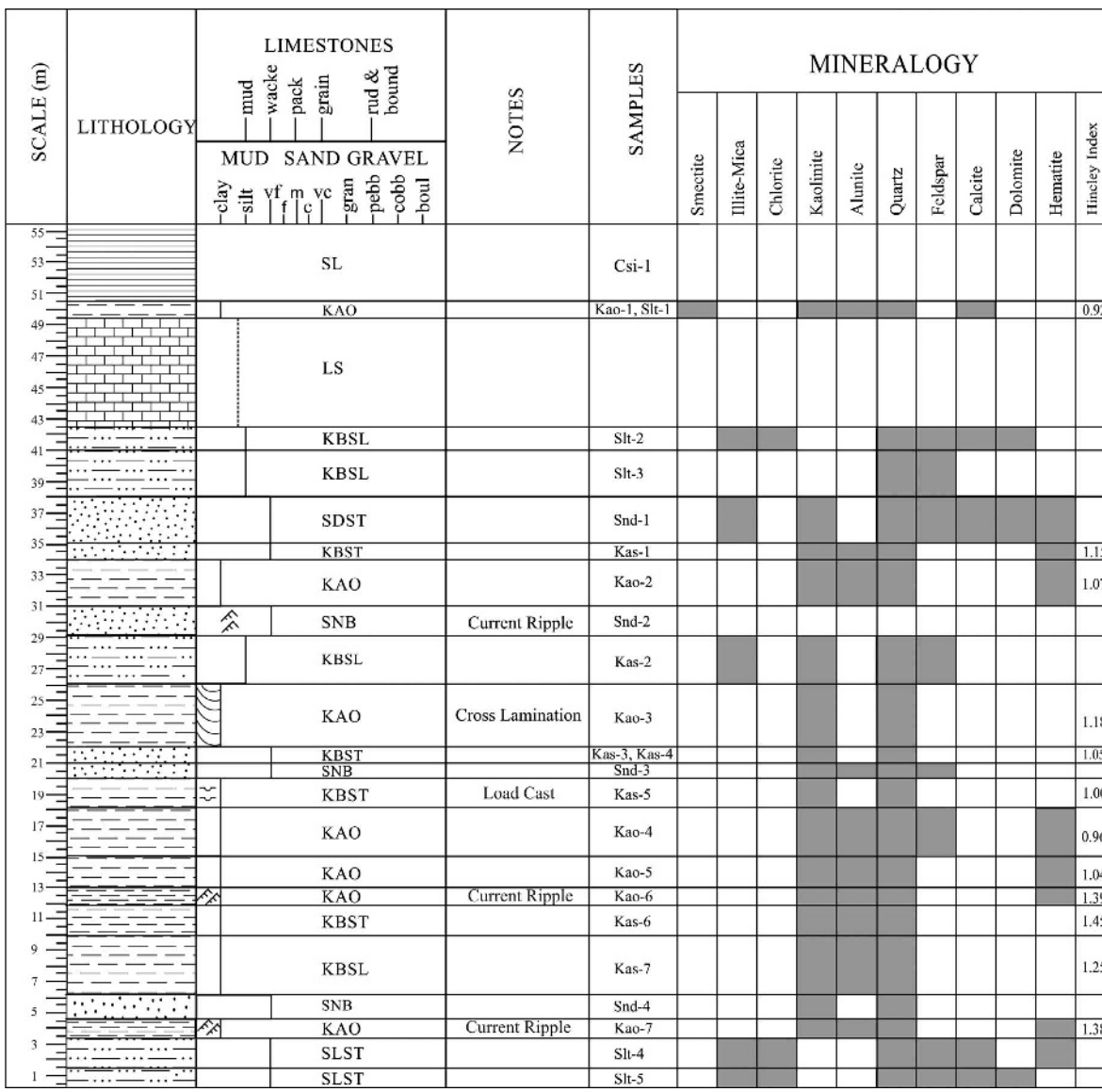

Figure 3. Lithology and mineral logs of the Çakmaktepe kaolin deposit, Banaz region. Abbreviations: siltstone (SLST), kaolin (KAO), sand bed (SNB), kaolinite-bearing siltstone (KBSL), kaolinite-bearing sandstone (KBST), sandstone (SDST), limestone (LS), and the silica layer (SL).

https://doi.org/10.1346/CCMN.2015.0630401 Published online by Cambridge University Press

(SNB), kaolinite-bearing siltstone (KBSL), kaolinite-bearing sandstone (KBST), sandstone (SDST), limestone (LS), and the silica layer (SL) can be distinguished from the bottom to the top (Figures 3, 4a). The siltstone consisted primarily of very fine silt, fine silt, and minor kaolinite at the KBSL level. The thickness of the siltstone

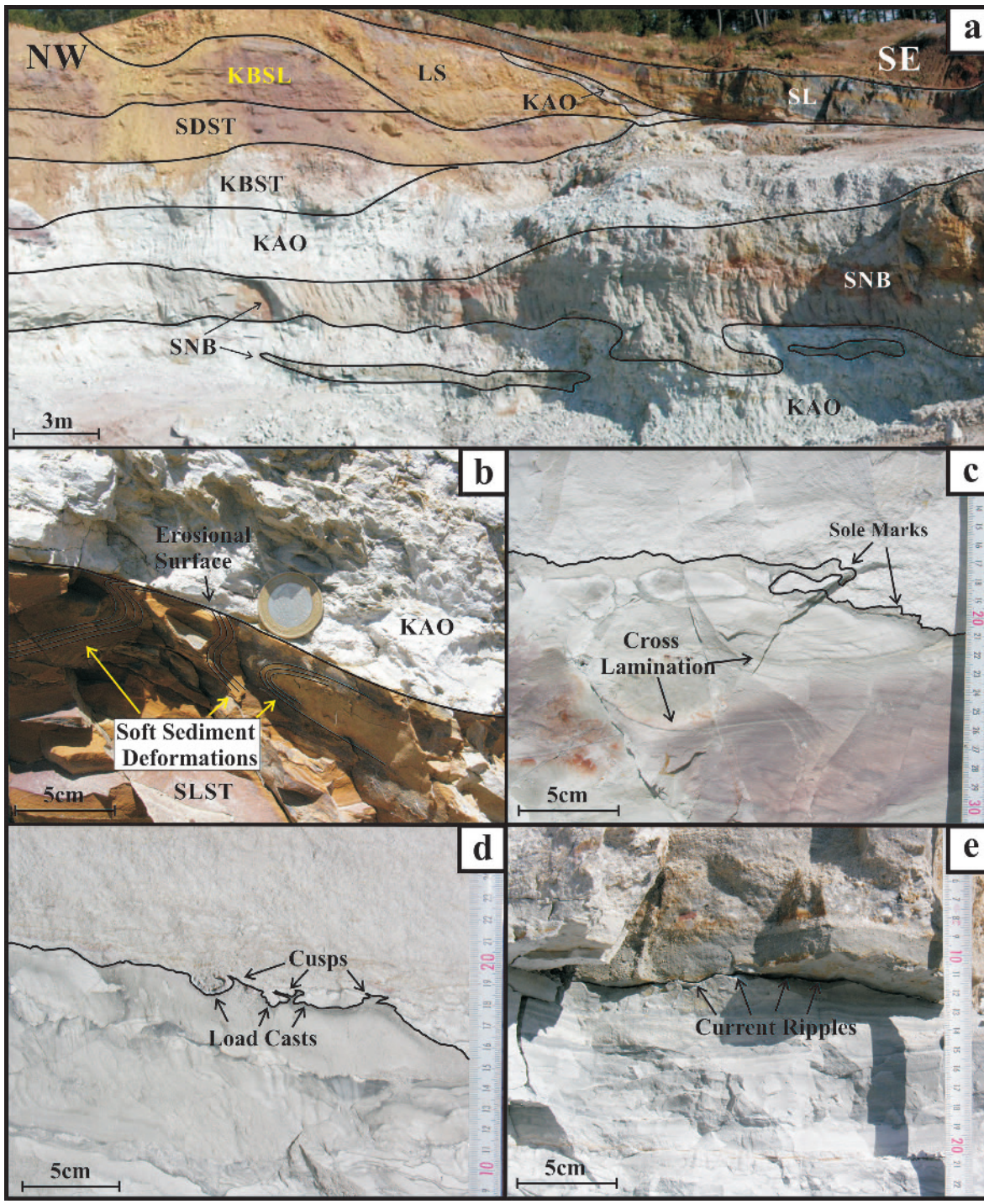

Figure 4. Outcrop photos of the Çakmaktepe kaolin deposit: (a) the open pit showing kaolin units in sedimentary rocks of Yeniköy; (b) the sharp contact between siltstones (SLST) and kaolin (KAO) levels and microfolds within the siltstones; (c) sole marks and trough cross laminations between kaolin and KBSL levels; (d) load casts and cusps between kaolin and KBSL levels; and (e) current ripples between kaolin and SNB levels.

https://doi.org/10.1346/CCMN.2015.0630401 Published online by Cambridge University Press

layers ranged from 1 to 3 m. Erosional surfaces and soft sediment deformation were observed at the contacts of the siltstones with kaolin (Figure 4b). The kaolin units were interbedded with the SNB, KBSL, and KBST intervals. The thicknesses of the kaolin layers ranged from 1.5 to 4 m. The grain sizes in the kaolin layers varied and generally decreased from the base to the top. Finer grain sizes typically result in darker kaolin layers. The lowest layer consisted of cream-colored kaolin with a gray kaolin layer above. Trough cross-lamination and tool marks were observed at the top of the light-gray and cream-colored kaolin layers (Figure 4c). The kaolin units were weakly consolidated, and the surfaces of kaolins of the KBST and SNB intervals were distinguished by load casts, cusps, and asymmetric current ripples (Figures 4d, 4e). The sand bed consisted primarily of 18−67 μm quartz grains (medium silt to very fine sand). The quartz grains were very angular and were loosely cemented with a kaolinitic matrix. The bed was interbedded with kaolin, KBST, and KBSL, and the thickness ranged from 1 to 3 m. The sandstone layer was composed of quartz, feldspar, muscovite, and minor rock fragments, with a thickness of ~3 m. The grain sizes in the sandstone layer ranged from 31 to 227 μm (coarse silt to fine sand) with very angular clasts. The KBST interval was located in the middle of the sequence and consisted mainly of quartz crystals, subordinate muscovite, feldspar, and lithic fragments. The sizes of components were between 68 and 683 μm (very fine sand to coarse sand), and kaolinite was identified as the matrix. The limestone (LS) layer, with a thickness of 5 m, was yellow and cream colored with a micritic texture. This level was composed of plaque-shaped strata and included minor clay components. The SL overlying the LS was a reddish brown to black fine-textured and brittle silica layer that consisted of microcrystalline quartz crystals. The silica level was distinct from the limestone levels, and silicification and replacement textures were not observed within the lower layers of the deposit. Lens-shaped kaolin levels (Kao-1) were observed along the boundary between the SL and LS layers.

Mineralogy

X-ray diffraction studies. The argillic alteration zones in the KBV were composed of acidic mineral assemblages and an intermediate alteration with similar mineralogical composition to Çakmaktepe kaolins (Table 1). Zonation of the minerals was recognized in the argillic alteration zones. Smectite (30−55%) was the major phyllosilicate present in the outer zones of the argillic alteration. The inner zone, which represents advanced alteration, was distinctive due to the presence of minor to moderately abundant kaolinite (10−40%) and minor smectite (12−15%). Illite-mica (Ilt-M), gypsum, alunite, quartz, feldspar, calcite, dolomite, and hematite were identified as subordinate minerals in all of the alteration zones (Table 1).

The mineral distributions in the kaolins and the KBS from various stratigraphic intervals in the Çakmaktepe deposit are shown in the litholog and mineral logs of the Çakmaktepe kaolin deposit (Figure 3). The common minerals identified at all levels included kaolinite, smectite, quartz, and feldspar, and some samples included illite-mica, calcite, and dolomite as secondary (Figure 5). The kaolins and KBS contained abundant kaolinite (55−70%), minor smectite (15%), and minor alunite (2−15%) and hematite (1−2%). Kaolinite abundances were inversely correlated with the quartz abundances in the kaolin units and the KBS interval. Larger kaolinite abundances were observed in the kaolin layers than in the KBS intervals. This variation in the kaolinite abundance was observed in all strata near the contacts between the kaolins and clastic sedimentary rocks. The light gray and gray kaolin intervals (Kao-4 and Kao-5, respectively), which contain sedimentary structures, contained more kaolinite than the KBST and KBSL intervals (Kas-6 and Kas-7). Minor smectite abundances were observed in the kaolin layer (Kao-1) at the top of the stratigraphic profile. The SLST layers in the lower portions were distinguished from other stratigraphic levels in the Çakmaktepe deposit because they contain minor to intermediate amounts of chlorite (20−25%), minor illite-mica (15%), and minor feldspar (5%) (Figure 5). Quartz (65−93%) was identified as a common detrital component in the SNB layers (Snd-2, Snd-3, and Snd-4). In addition, minor and intermediate kaolinite (5−25%) and minor calcite (5−15%) abundances were detected in these layers. The SL layer consisted of 100% quartz minerals. The alunite contents and the Hinckley crystallinity indices (HI) decreased gradually from the bottom to the top of the stratigraphic profile.

Diffraction intensities at 7.17, 4.48, 3.58, 2.50, and 2.35 Å are characteristic of kaolinite in kaolin units. Sharp diffraction peaks at 7.17 and 3.58 Å and the presence of peaks at 4.18 and 3.87 Å indicate the presence of ordered kaolinite (MacEwan and Wilson, 1980; Wilson, 1987; Arslan *et al.*, 2006). The kaolinites in the Çakmaktepe region (except for samples Kao-1 and Kao-7) were observed to have HI values >1.00, which indicated a high degree of crystallization (Table 1). Well crystallized kaolinites are formed from hydrothermal alteration, whereas the presence of sedimentary kaolinites with low, moderate, and high crystallization is related to supergene alteration (Patterson and Murray, 1975; Galan *et al.*, 1977; Nakagawa *et al.*, 2006).

The peak at 7.17 Å in the kaolin and the KBS samples remained unchanged by the ethylene glycol treatment. This peak collapsed completely after heating to 550ºC due to dehydroxylation (Figure 6). The formamide test was applied to highlight the occurrence of the kaolinite minerals in the Çakmaktepe samples and to differentiate kaolinite from halloysite. These minerals can be differentiated from each other by d_{001} diffraction because the d_{001} diffraction of kaolinite occurs at 7.2 Å and that of

https://doi.org/10.1346/CCMN.2015.0630401 Published online by Cambridge University Press

Table 1. Semi-quantitative analysis results (%) and Hinckley crystallinity index value of samples from the study area.

Sample code	Sample type	Sme	Ilt-M	Chl	Gp	Kln	Alu	Crs-Opl	Qz	Fsp	Cal	Dol	Hem	HI
Csi-1	SL	0	0	0	0	0	0	0	100	0	0	0	0	–
Kao-1	KAO	15	0	0	0	70	3	0	10	0	1	0	1	0.92
Slt-1	SLST	10	30	25	0	0	0	0	20	5	2	0	8	–
Slt-2	KBSL	0	10	0	0	60	0	0	20	3	5	2	0	–
Snd-1	SDST	0	5	10	0	0	0	0	50	10	20	5	0	–
Kas-1	KBST	0	0	0	0	60	3	0	35	0	0	0	2	1.15
Kao-2	KAO	0	0	0	0	65	2	0	33	0	0	0	0	1.07
Snd-2	SNB	0	0	0	0	20	0	0	65	0	15	0	0	–
Kas-2	KBSL	0	5	0	0	60	2	0	25	5	0	3	0	–
Kao-3	KAO	0	0	0	0	70	3	0	20	5	2	0	0	1.18
Kas-3	KBST	0	0	0	0	60	3	0	35	0	0	0	2	1.05
Kas-4	KBST	0	0	0	0	60	5	0	35	0	0	0	0	1.17
Snd-3	SNB	0	0	0	0	25	0	0	70	0	5	0	0	–
Kas-5	KAO	0	3	0	0	60	10	0	20	5	0	2	0	1.00
Kao-4	KAO	0	0	0	0	70	5	0	20	3	2	0	1	0.96
Kao-5	KAO	0	0	0	0	65	3	0	30	0	0	0	2	1.04
Kao-6	KAO	0	0	0	0	70	15	0	15	0	0	0	0	1.39
Kas-6	KBST	0	0	0	0	55	5	0	40	0	0	0	0	1.45
Kas-7	KBSL	0	0	0	0	60	5	0	35	0	0	0	0	1.25
Snd-4	SNB	0	0	0	0	5	0	0	93	0	0	0	2	–
Kao-7	KAO	0	0	0	0	70	13	0	15	0	0	0	2	1.38
Slt-4	SLST	0	15	20	0	0	0	0	45	5	5	0	10	–
Slt-5	SLST	0	15	25	0	0	0	0	50	5	2	3	0	–
Ttf-1	TUFF	35	10	0	0	0	0	20	15	20	0	0	0	–
Oan-2	TAN	15	5	0	0	10	2	0	25	35	2	3	3	–
Oan-3	TAN	0	20	0	0	40	0	0	40	0	0	0	0	–
Oan-5	TAN	30	10	0	0	0	0	15	15	25	2	3	0	–
San-2	TAN	15	10	0	0	15	1	0	25	30	1	2	1	–
San-3	TAN	12	13	0	0	15	2	0	25	30	0	2	1	–
San-6	TAN	50	10	0	15	0	5	0	10	10	0	0	0	–
San-9	TAN	55	2	0	5	0	15	10	3	5	0	0	5	–

Mineral-name abbreviations after Whitney and Evans (2010).
HI: Hinckley crystallinity index, SL: silica layer, KBST: kaolinite-bearing sandstone, KBSL: kaolinite-bearing siltstone, SLST: siltstone, SDST: sandstone, SNB: sand bed, and TAN: trachyandesite.

halloysite occurs at 10.0 Å (Churchman *et al.*, 1984). In the present study, the d_{001} diffraction observed at 7.2 Å in the XRD analysis performed after the formamide test indicated the existence of kaolinite in the Çakmaktepe samples (Figure 6).

SEM-EDX determinations. Platy kaolinite crystals with pseudo-hexagonal forms were observed in all of the kaolin and KBS samples (Figure 7a). Large vermiform kaolinite booklets and stacks were absent, however. The kaolinite crystals exhibited an edge-to-face arrangement with irregular outlines and crystals of 0.4−2.6 μm. A few kaolinite crystals were broken and showed rounded morphologies. The crystal size of the kaolinites was related indirectly to the kaolinite contents in the different layers of the Çakmaktepe deposit. The crystal sizes ($\leqslant$1 μm) of the kaolinites in the kaolin layers were smaller than those in the KBS levels (> 1 μm). Subhedral alunite crystals were observed at the bottom (Kao-7) of the deposit (Figure 7b). The lower level (Kao-1) of the deposit, however, contained smectite crystals in the form of flakes (Figure 7c). The kaolinite particles cling tightly to the subhedral and low-sphericity quartz crystals and muscovite particles with platy crystals and books (Figures 7d,e,f). Microcrystalline quartz was present within the silica intervals in the uppermost portions of the kaolin deposits. In certain parts, the quartz minerals varied in size from 2 to 6 μm (Figure 7g, 7h). No textural or microscopic evidence was noted for dissolution-precipitation or replacement mechanisms of the muscovite minerals in the kaolin intervals. The compositional differences were significant between the muscovite and kaolinite crystals in the microchemical analytical (EDS) studies. The lack of Fe, lowest Mg, and highest Al contents characterized the muscovite in kaolin layers (Figure 8a). The aluminum, silica, potassium, and sulfate abundances of the Kao-7 (Spectrum 2) reflected the alunite content in Kao-7 (Figure 8b). The aluminum, silica, calcium, and magnesium contents in Kao-1 (Spectrum 2) were related to the smectite (Figure 8c).

https://doi.org/10.1346/CCMN.2015.0630401 Published online by Cambridge University Press

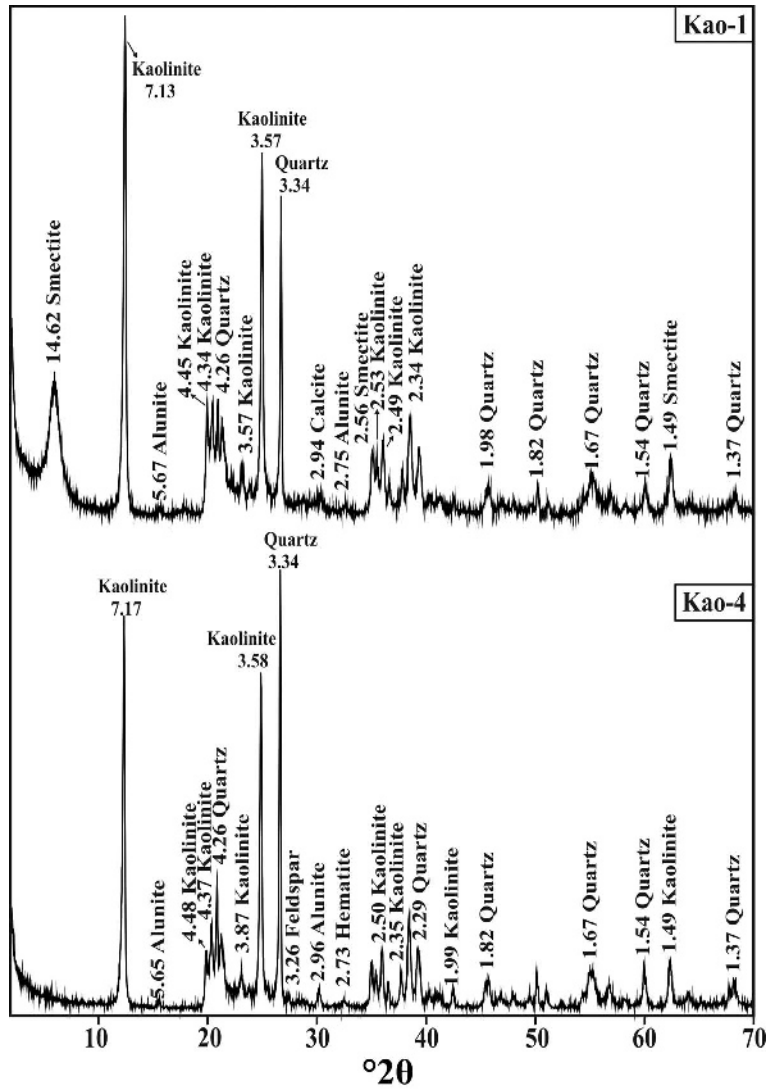

Figure 5. Representative powder XRD patterns of bulk samples of the Çakmaktepe kaolins.

Geochemistry

Geochemistry of kaolinization in Karaboldere Volcanics (KBV). Çakmaktepe kaolins were alteration products of KBV from Lower–Middle Miocene volcanic rocks in western Anatolia. Elemental behavior during alteration was determined using major- and trace-element analyses (Table 2).

The Zr/TiO_2 *vs.* Nb/Y diagram produced by Winchester and Floyd (1977) was used to discriminate between the magmatic compositions (Pearce *et al.*, 1984) and to identify the precursor materials of the kaolins (Dill *et al.*, 1997; Arslan *et al.*, 2006; Karakaya, 2009) and bentonites (Christidis *et al.*, 1995; Yıldız and Kuscu, 2004; Yıldız and Dumlupunar, 2009). This technique can be used because Zr, Nb, Y, and Ti show immobile behavior during various petrological processes (*i.e.* hydrothermal alteration, metamorphism, weathering, and sedimentation). The Zr/TiO_2 *vs.* Nb/Y discrimination diagram showed that the kaolins and volcanic rocks plotted in the andesite and trachyandesite fields (Figure 9). The sedimentary origins of kaolin deposits in the Çakmaktepe region could therefore be attributed to andesitic and trachyandesitic source rocks associated with KBV.

The elemental abundance of the fresh/unaltered volcanic samples was compared with that of the altered samples in an attempt to identify elemental behaviors during alteration. The TiO_2 and Al_2O_3 were immobile or minimally mobile, respectively, in all alteration zones (Figure 10), and SiO_2 was enriched both in the smectitic zone (Oan-7 and San-6) and in the kaolinitic samples (Oan-3, Oan-4, and San-3). Significant leaching was observed for CaO, Na_2O, and Fe_2O_3 in altered volcanics relative to fresh/unaltered rocks, especially in the kaolinitic zones compared with the smectitic zones.

https://doi.org/10.1346/CCMN.2015.0630401 Published online by Cambridge University Press

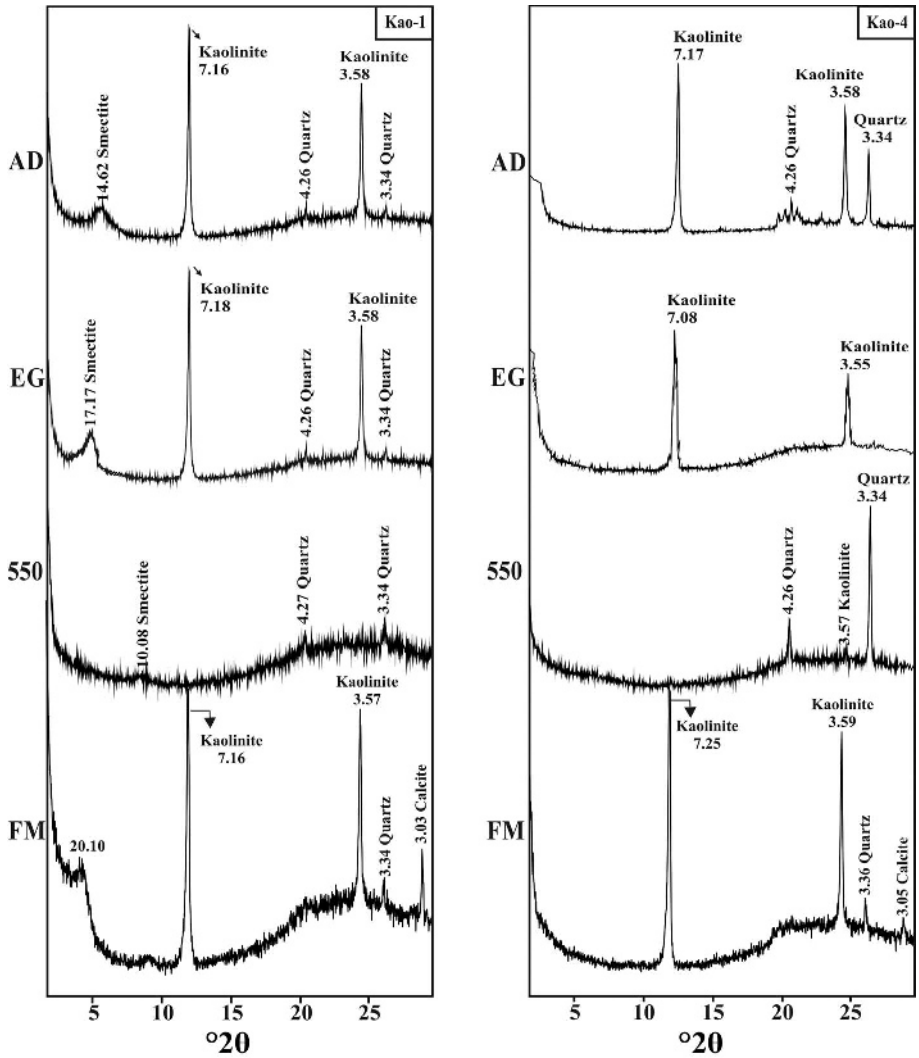

Figure 6. Representative XRD patterns of the clay fraction of Çakmaktepe kaolins. Abbreviations: AD – air dried; EG – ethylene glycolated; 550 – heated at 550ºC; and FM – treated with formamide.

Enrichments of K_2O and MgO were observed in the smectitic zone; these elements were depleted significantly, however, in the kaolinitic zone. In kaolinitic alteration, primary Ca-, Na-, and K-bearing silicates are replaced by Al-rich clay minerals. The Na^+ and K^+ ions that occupy the interlayer positions in the smectite are readily ion-exchanged for dissolved Ca^{2+} (Ross and Hendricks, 1945). The roles of the LILEs (large ion lithophile elements), including Ba, Rb, and Sr, are closely related to the rock-forming minerals in the the parent rock. The Sr content is decreased by the alterations of K- and Ca-bearing minerals. The breakdown of K-feldspar and hornblende results in a reduction in the amount of Ba, Rb, and K_2O (Arslan *et al.* 2006; Karakaya, 2009). In the study area, the Rb content was increased in the smectite zone (Oan-5 and Oan-7), and the amounts of Ba, Rb, and Sr (Oan-3, Oan-4, and San-3) in the kaolinitic zone decreased (Figure 10). Two explanations are proposed for the mobility of HFS elements (*e.g.* Hf, Nb, Ta, Zr, and Y) during different geological processes (magmatic, metamorphic, and hydrothermal). According to Floyd and Winchester (1978), Corfu and Davis (1991), Salvi *et al.* (2000), and Jiang *et al.* (2003), HFS elements are immobile. Others (Saunders *et al.*, 1980; Jiang, 2000;

Figure 7 (*facing page*). SEM images of Çakmaktepe kaolins and the silica layer: (a) platy kaolinite crystals (Kln) with pseudohexagonal borders; (b) subhedral alunite (Alu) crystals with kaolinites; (c) smectite (Sme) crystals in the form of flakes; (d,e) kaolinite crystals surrounding cleaved sheets of muscovite (Ms); (f) subhedral quartz crystals (Qz) accompanied by kaolinite; (g,h) octahedral microcrystalline quartz minerals.

https://doi.org/10.1346/CCMN.2015.0630401 Published online by Cambridge University Press

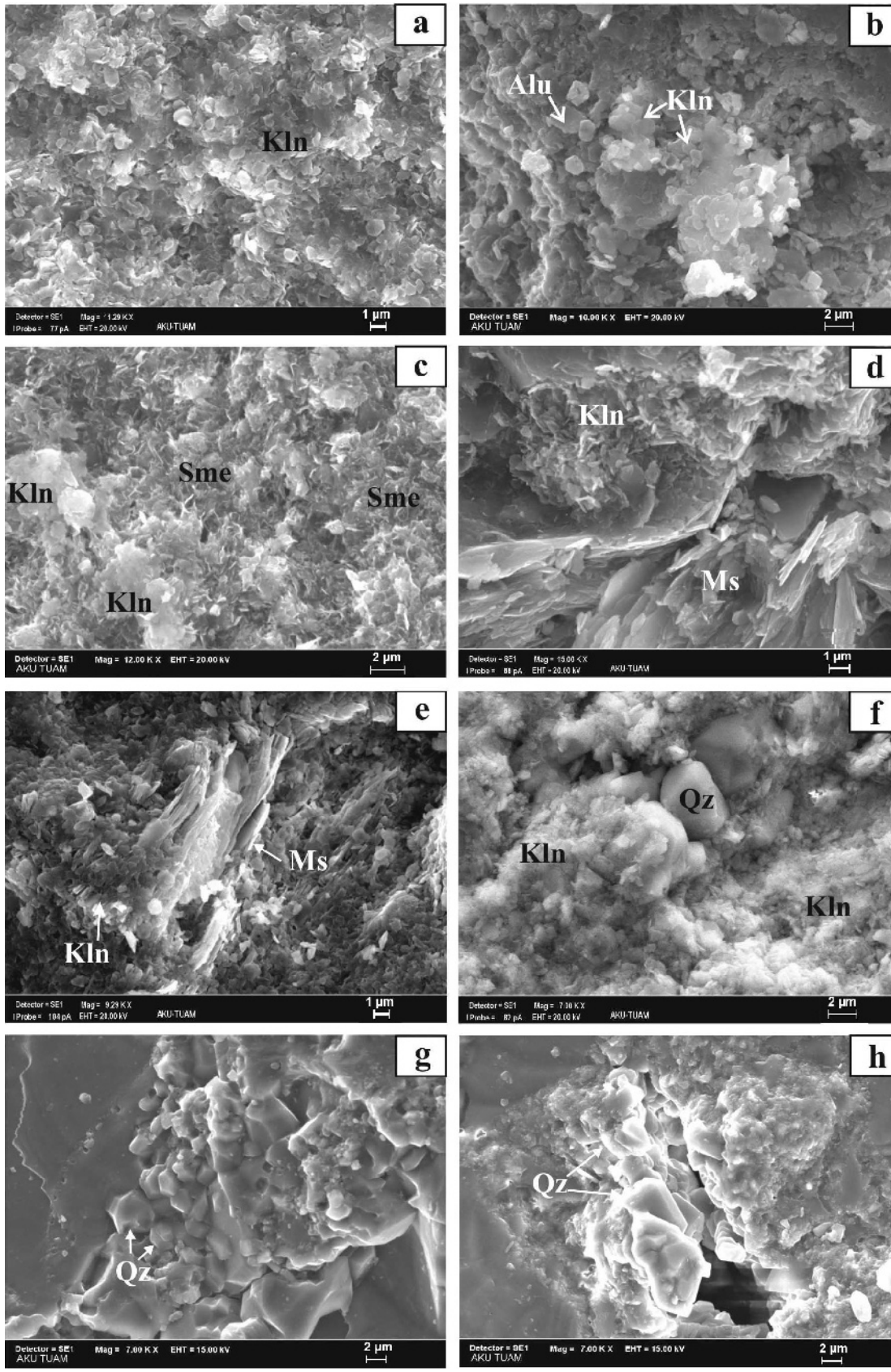

https://doi.org/10.1346/CCMN.2015.0630401 Published online by Cambridge University Press

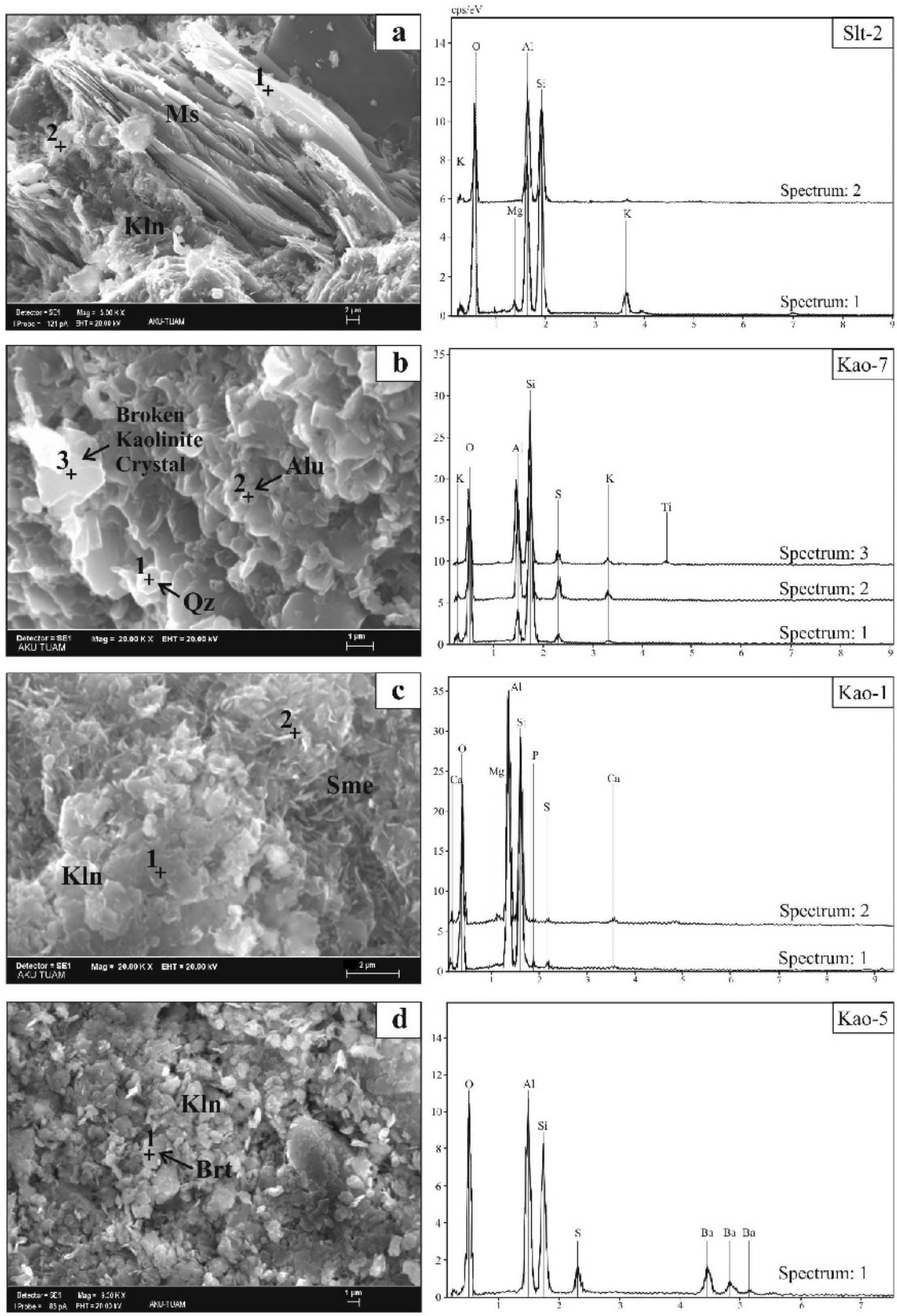

Figure 8. EDS spectra of Çakmaktepe kaolins. Abbreviations after Whitney and Evans (2010).

https://doi.org/10.1346/CCMN.2015.0630401 Published online by Cambridge University Press

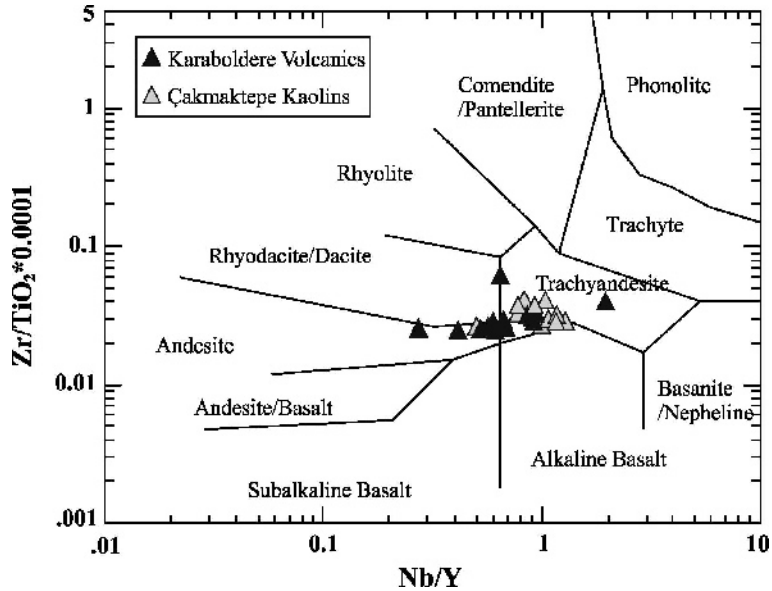

Figure 9. The discrimination plot of Zr/TiO_2 *vs*. Nb/Y for the Karaboldere volcanics (KBV) and the Çakmaktepe kaolins.

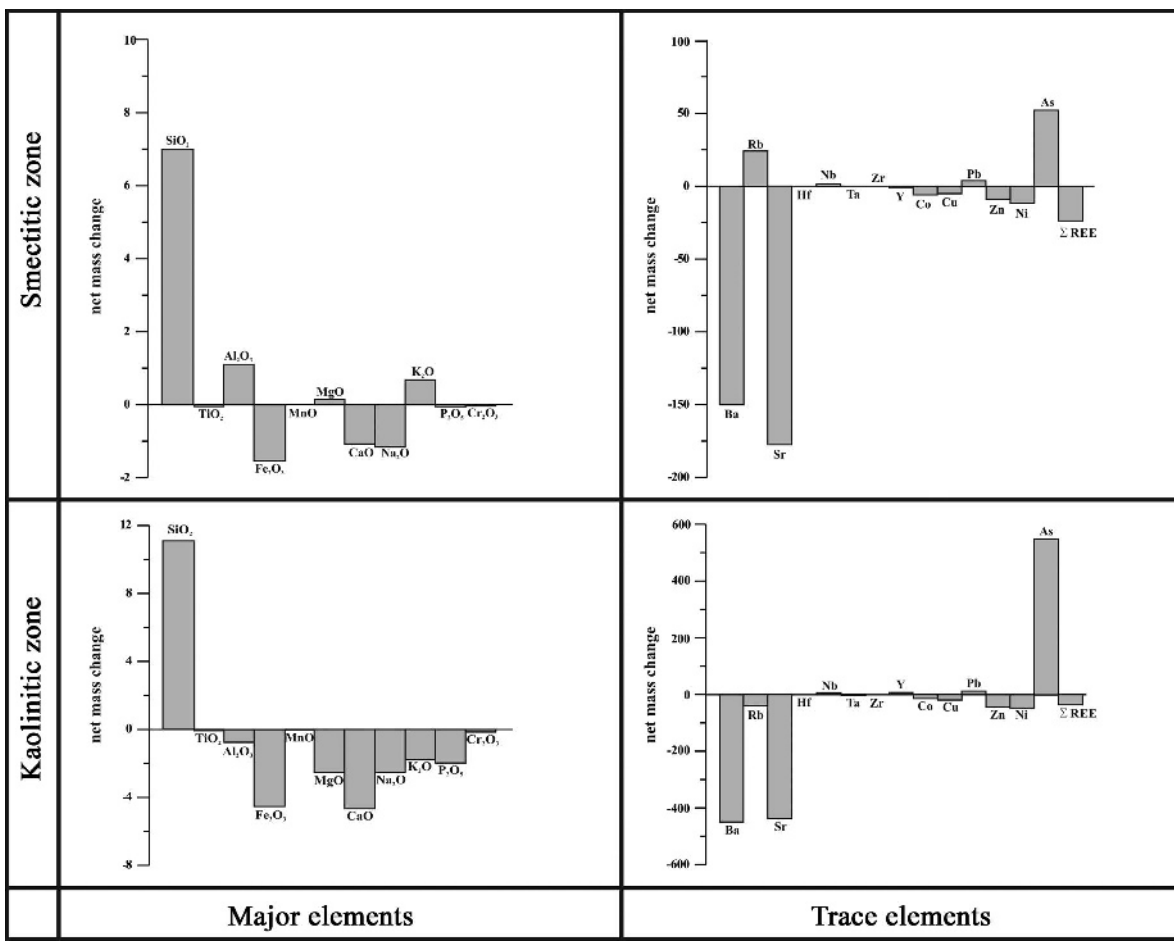

Figure 10. Mass changes of major elements (g) and trace elements (ppm) during alteration of Karaboldere volcanics (KBV).

https://doi.org/10.1346/CCMN.2015.0630401 Published online by Cambridge University Press

Table 2. Whole-rock chemical composition of argillic alteration zones in Karaboldere volcanics (SiO_2 to S in wt.%; Ba to Sb in ppm).

Sample code Sample type	Ran-1* TAN	Oan-1* TAN	Oan-2* TAN	Tan-2* TAN	Kan-1* TAN	San-1* TAN	Oan-3 TAN	Oan-4 TAN	Oan-5 TAN
SiO_2	60.50	61.30	61.12	61.92	58.08	63.18	75.44	75.54	67.19
TiO_2	0.52	0.54	0.53	0.59	0.52	0.63	0.57	0.52	0.59
Al_2O_3	13.26	13.64	14.11	13.45	11.94	14.77	13.51	14.01	14.13
Fe_2O_3	4.83	4.99	4.93	5.94	4.88	5.68	1.49	1.06	1.76
MnO	0.11	0.07	0.08	0.08	0.09	0.04	0.01	0.01	0.01
MgO	3.69	3.07	2.47	3.97	4.19	1.53	0.46	0.36	1.15
CaO	5.36	4.63	4.23	5.46	6.65	3.74	0.28	0.07	1.34
Na_2O	2.48	2.52	2.60	2.32	1.75	2.61	0.13	0.04	1.42
K_2O	2.45	2.83	3.01	2.31	1.84	3.22	0.99	1.02	3.63
P_2O_5	0.13	0.13	0.11	0.14	0.09	0.16	0.01	0.04	0.04
Cr_2O_3	0.02	0.02	0.01	0.04	0.02	0.03	0.01	0.01	0.02
Total S	0.02	0.02	0.05	0.02	0.02	0.02	0.27	0.31	0.04
LOI	6.40	6.10	6.40	3.50	9.80	4.20	7.10	7.3	8.60
Total	99.81	99.81	99.63	99.72	99.80	99.77	99.95	99.95	99.85
Ba	621.00	672.00	724.00	907.00	551.00	897.00	474.00	325	768.00
Co	14.00	14.60	12.00	18.90	12.90	16.60	1.30	0.9	3.80
Cs	3.50	6.00	6.40	7.80	3.30	7.70	7.60	8.4	5.30
Hf	3.60	4.40	3.90	4.60	3.40	5.00	5.30	4.5	5.50
Nb	12.30	11.70	13.40	11.70	10.90	13.10	14.50	13.5	13.90
Rb	89.80	98.20	108.40	77.20	68.60	112.50	48.90	65.6	123.60
Sr	381.40	380.10	1708.30	567.30	375.60	476.50	42.50	19.1	269.80
Ta	1.00	1.00	0.90	0.90	0.70	1.00	1.00	0.8	1.20
Th	11.60	12.30	13.60	14.30	11.10	16.70	13.80	14.2	15.80
U	4.60	4.70	4.40	5.00	3.80	5.70	4.00	4.6	8.30
V	94.00	95.00	89.00	106.00	89.00	99.00	87.00	68	48.00
W	2.50	1.90	1.90	1.50	2.00	1.90	5.60	3.5	2.30
Zr	136.20	152.80	148.30	150.70	136.60	155.00	179.70	145.7	186.70
Y	18.40	19.60	19.80	22.30	18.60	18.20	16.30	31.7	15.10
La	29.50	32.30	33.40	34.10	25.60	40.50	29.30	30	24.60
Ce	52.00	57.30	55.20	66.90	48.10	73.30	52.60	55.4	50.60
Pr	6.08	6.81	6.73	7.67	5.67	8.13	5.89	5.85	5.68
Nd	21.00	24.00	22.50	27.60	21.60	30.10	22.70	21.3	22.50
Sm	3.90	4.33	4.03	4.69	3.95	5.07	3.53	3.81	3.45
Eu	0.91	0.96	0.91	1.12	0.85	1.01	0.84	1	0.76
Gd	3.36	3.68	3.60	4.46	3.50	3.98	3.35	3.99	3.19
Tb	0.56	0.62	0.60	0.71	0.55	0.64	0.49	0.76	0.46
Dy	3.24	3.29	3.45	4.18	3.15	3.50	2.70	4.78	2.54
Ho	0.63	0.66	0.65	0.79	0.61	0.70	0.59	1.02	0.51
Er	1.87	1.92	1.85	2.16	1.83	2.02	1.70	3.03	1.49
Tm	0.30	0.32	0.35	0.32	0.28	0.31	0.27	0.46	0.26
Yb	1.80	2.11	1.96	2.09	1.75	2.11	1.80	3.05	1.53
Lu	0.28	0.32	0.32	0.33	0.27	0.30	0.28	0.45	0.26
Mo	2.10	1.90	3.30	3.20	0.80	0.80	2.40	4.1	1.20
Cu	20.60	13.60	14.40	28.60	19.60	21.60	3.60	3.4	11.50
Pb	13.90	10.20	9.00	11.30	11.70	4.80	32.70	16.8	8.40
Zn	49.00	56.00	52.00	36.00	42.00	42.00	8.00	4	23.00
Ni	46.60	53.40	24.90	50.20	52.10	41.80	9.80	9.9	15.90
As	8.00	7.20	2.80	3.50	12.00	3.60	594.70	389.8	251.90
Sb	0.20	0.30	0.30	0.40	0.10	0.70	1.80	2.1	0.10

TAN (trachyandesite), and marked samples (*) are fresh/unaltered.

Jiang *et al.*, 2005; Karakaya, 2009; Karakaya *et al.*, 2012), however, suggested that HFS elements are mobile and that the mobility of HFS elements is controlled by various actors, such as *P-T* conditions, pH, and solution chemistry during alteration processes. In the study area, HFS elements showed relatively immobile behavior in different alteration zones at the Kozören district.

Similar element mobility occurred for the LILE (large-ion lithophile elements; *e.g.* Ba, Sr, K), and HFS elements were observed in the hydrothermally formed

https://doi.org/10.1346/CCMN.2015.0630401 Published online by Cambridge University Press

Table 2. Continued.

Sample code Sample type	Oan-7 TAN	Tan-3 TAN	San-2 TAN	San-3 TAN	San-6 TAN	San-8 TAN	San-9 TAN	Ttf-1 TUFF
SiO_2	57.3	55.89	61.36	68.54	60.48	64.62	32.37	65.66
TiO_2	0.53	0.46	0.46	0.48	0.49	0.59	0.28	0.26
Al_2O_3	12.74	13.28	13.21	13.78	13.97	12.56	4.25	13.34
Fe_2O_3	4.71	4.64	3.73	4.15	3.16	3.18	30.34	2.29
MnO	0.14	0.03	0.09	0.06	0.02	0.01	0.01	0.04
MgO	3.23	3.65	2.19	0.89	2.11	1.56	0.59	1.46
CaO	5.7	1.75	4.19	0.57	2.01	1.27	0.72	1.64
Na_2O	1.84	0.23	0.57	0.64	0.84	1.09	1.76	1.36
K_2O	2.92	3.18	4.82	5.15	2.75	3.04	2.01	3.87
P_2O_5	0.12	0.09	0.11	0.13	0.12	0.05	0.08	0.05
Cr_2O_3	0.01	0.01	0.01	0.00	0.01	0.01	0.01	0.01
Total S	0.02	0.02	0.08	0.03	0.45	0.50	5.86	0.02
LOI	10.6	16.60	9.10	5.50	13.90	11.90	27.30	9.90
Total	99.83	99.80	99.81	99.84	99.84	99.83	99.76	99.89
Ba	758	684.00	807.00	889.00	630.00	737.00	509.00	471.00
Co	12.2	11.50	8.20	8.20	16.60	3.10	1.70	3.80
Cs	4.6	21.20	10.10	10.30	2.00	7.30	5.00	21.90
Hf	4.2	3.90	4.20	4.10	3.90	5.60	2.50	4.70
Nb	12.3	11.40	12.80	14.20	11.80	11.80	6.30	18.00
Rb	102.6	101.90	205.10	222.50	74.50	109.10	72.70	215.60
Sr	377.3	328.70	234.30	99.60	178.40	282.30	1089.10	166.40
Ta	1	0.90	1.20	1.30	1.10	1.10	0.50	1.40
Th	15.1	10.60	16.60	17.00	14.80	11.80	6.00	24.90
U	4.1	2.50	11.20	5.00	7.00	3.60	2.80	7.20
V	42	70.00	80.00	78.00	68.00	49.00	36.00	27.00
W	1.1	0.90	2.00	2.30	1.30	3.10	1.60	2.00
Zr	147.4	143.40	139.20	135.50	130.60	201.60	82.80	128.30
Y	21	13.10	19.80	20.50	14.70	5.90	7.80	27.30
La	32.2	26.10	36.10	37.70	28.20	28.00	13.70	25.40
Ce	63.2	51.80	65.90	68.80	55.40	43.80	22.80	51.90
Pr	7.12	5.71	6.90	7.36	5.93	3.62	2.96	5.85
Nd	27.2	20.40	26.20	27.90	21.20	10.80	12.20	19.80
Sm	4.68	3.26	4.32	4.55	3.74	1.81	1.86	3.87
Eu	1.01	0.81	0.96	0.98	0.75	0.38	0.39	0.59
Gd	4.64	3.19	3.89	3.92	3.33	1.39	1.59	4.30
Tb	0.69	0.48	0.63	0.64	0.52	0.21	0.24	0.75
Dy	3.78	2.55	3.19	3.27	2.70	0.93	1.36	4.65
Ho	0.71	0.47	0.69	0.74	0.58	0.21	0.27	0.93
Er	2.1	1.27	2.08	2.18	1.78	0.73	0.79	2.72
Tm	0.31	0.20	0.33	0.32	0.24	0.11	0.13	0.44
Yb	2.1	1.26	2.05	2.27	1.67	0.80	0.88	2.99
Lu	0.29	0.19	0.28	0.35	0.24	0.13	0.13	0.46
Mo	0.6	0.60	1.40	1.90	0.50	1.40	152.10	1.00
Cu	26.1	12.20	17.40	13.50	15.60	3.00	7.90	7.60
Pb	7.5	14.00	12.80	25.20	16.30	7.80	15.50	13.90
Zn	61	40.00	43.00	56.00	17.00	9.00	11.00	21.00
Ni	34.6	52.70	9.20	11.90	37.00	4.70	4.80	18.60
As	14.3	4.30	11.40	44.40	36.10	105.00	2738.20	2.20
Sb	0.9	0.20	0.30	1.20	0.80	0.30	6.50	0.10

TAN (trachyandesite), (TUFF): tuff.

alteration zones in Lesbos, Greece (Kelepertsis and Esson, 1987), in Erenler Dağı (Karakaya, 2009), Eastern Pontides (Karakaya *et al*., 2012), and in the sedimentary kaolin deposits in the Şile region, Turkey (Ece and Nakagawa, 2003). The total amount of As increased significantly during the progressive alteration. The abundances of transition metals, such as Co, Cu, Pb, Zn and Ni, in the altered samples were the most important indicators for determining the origins of the pore solutions relative to the parent rocks (Oan-1, Oan-2, and San-1) (Yalçın and Gümüşer, 2000) because element enrichment in clays during alteration results from

https://doi.org/10.1346/CCMN.2015.0630401 Published online by Cambridge University Press

structural incorporation, adsorption, and co-precipitation with secondary phases. (Zielinski, 1982). The Pb was enriched four- to fifteen-fold, and Co, Cu, Zn, and Ni were moved from the smectitic to the kaolinitic zones. The enrichment of Pb indicated precipitation by means of channeling of the hydrothermal solutions through ultramafic sources. The ultramafic rocks below the Yeniköy formation have been noted from geothermal drillings in the Hamamboğazı region and 20 km SW of the study area (MTA, 2005).

The chondrite-normalized *REE* patterns showed enrichment of the light rare earth elements (*LREE*) relative to C1 chondrites. Smectitic and kaolinitic zone samples all contain lower *REE* abundances than the fresh/unaltered volcanics. The *HREE* abundances in the kaolinitic zone are greater than in the smectitic zone or in the fresh/ unaltered volcanics. Slightly negative Eu anomalies occur: Eu/Eu* = 0.69−0.74 in fresh/unaltered volcanics, 0.44−0.77 in the smectitic zone, and 0.75−0.79 in the kaolinitic zone (Figure 11). The $(La/Sm)_{cn}$, $(Gd/Yb)_{cn}$, and $(La/Yb)_{cn}$ ratios were calculated to explain the fractionation of the *REE* during hydrothermal alteration. Specifically, *LREE* fractionation was calculated based on the $(La/Sm)_{cn}$, and *HREE* fractionation was calculated based on $(Gd/Yb)_{cn}$. The depletion of the *LREE* with respect to *HREE* was quantified as $(La/Yb)_{cn}$. Minor changes were observed in the *LREE* and *HREE* fractionations and in the $(La/Yb)_{cn}$ ratio of fresh/unaltered volcanics, smectitic, and kaolinitic zone. The *LREE* and *HREE* fractionation was [$(La/Sm)_{cn}$ = 4.69−5.16; $(Gd/Yb)_{cn}$ = 1.44−1.76] for fresh/unaltered volcanics, [$(La/Sm)_{cn}$ = 4.24−5.17; $(Gd/Yb)_{cn}$ = 1.19−2.09] for the smectitic zone, and [$(La/Sm)_{cn}$ = 5.08−5.36; $(Gd/Yb)_{cn}$ = 1.08−1.54] for the kaolinitic zone. The $(La/Yb)_{cn}$ ratio ranged from 10.98 to 13.77 in the fresh/unaltered volcanics, from 6.09 to 14.86 in the smectitic zone, and from 7.06 to 11.68 in the kaolinitic zone. The Eu anomaly may indicate origin, mobility, or fractionation. Eu^{2+} is mobile and removed from feldspar in parent rocks by hydrothermal fluids (Honty *et al*., 2008; Karakaya *et al*., 2012; Genna *et al*., 2014). In the evolution of magmatic rocks, the negative Eu anomaly reflects plagioclase fractionation in source rocks (Temizel and Arslan, 2009; Maurice *et al*., 2013).

Geochemistry of the Çakmaktepe kaolins. The major and trace elements and $\delta^{18}O$ values were plotted as a function of the stratigraphy in the litholog and the chemologs of the Çakmaktepe kaolin deposit (Figure 12, Table 3). SiO_2 and Al_2O_3 were identified as important components of the kaolins and kaolinite-bearing samples (Table 2). SiO_2 abundances in the kaolins were smaller (41.09−59.39 wt.%) than those of the KBSL and KBST intervals (60.96−66.91 wt.%). The SiO_2 abundnace was related to the predominance of medium silt-size and very fine sand-size quartz and increased progressively toward the sand beds (Snd-3 and Snd-4). The behavior of the Al_2O_3 was opposite that of silica and decreased gradually from the kaolins (26.74−31.90 wt.%) to the KBSL and KBST levels (19.27−23.99 wt.%). When high Al_2O_3 and low SiO_2 abundances were observed in the light gray and gray kaolin levels (Kao-4, Kao-5, and Kao-6) with sedimentary structures, the SLST (Slt-4 and Slt-5) and SDST (Snd-1) intervals were distinguished by their low Al_2O_3 and high SiO_2 contents (Figure 11).

The TiO_2 content in the kaolins and the KBS ranged from 0.24 to 0.95 wt.% and from 0.22 to 0.91 wt.%, respectively. TiO_2 was the key component that constrained the origin of the kaolins because it was generally <1.00 wt.% in the hypogene kaolins and became concentrated in the supergene kaolins and the sedimentary Georgia kaolins (6 wt.%) in the Coastal Plain region in the southeastern USA (Hurst and Pickering, 1997). The TiO_2 abundance increased by up

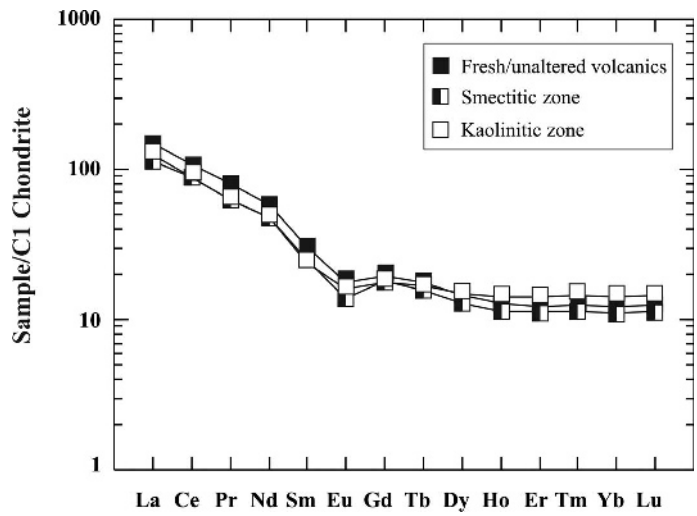

Figure 11. Chondrite-normalized abundances of average *REE* for the Karaboldere volcanics (KBV) and the Çakmaktepe kaolins.

https://doi.org/10.1346/CCMN.2015.0630401 Published online by Cambridge University Press

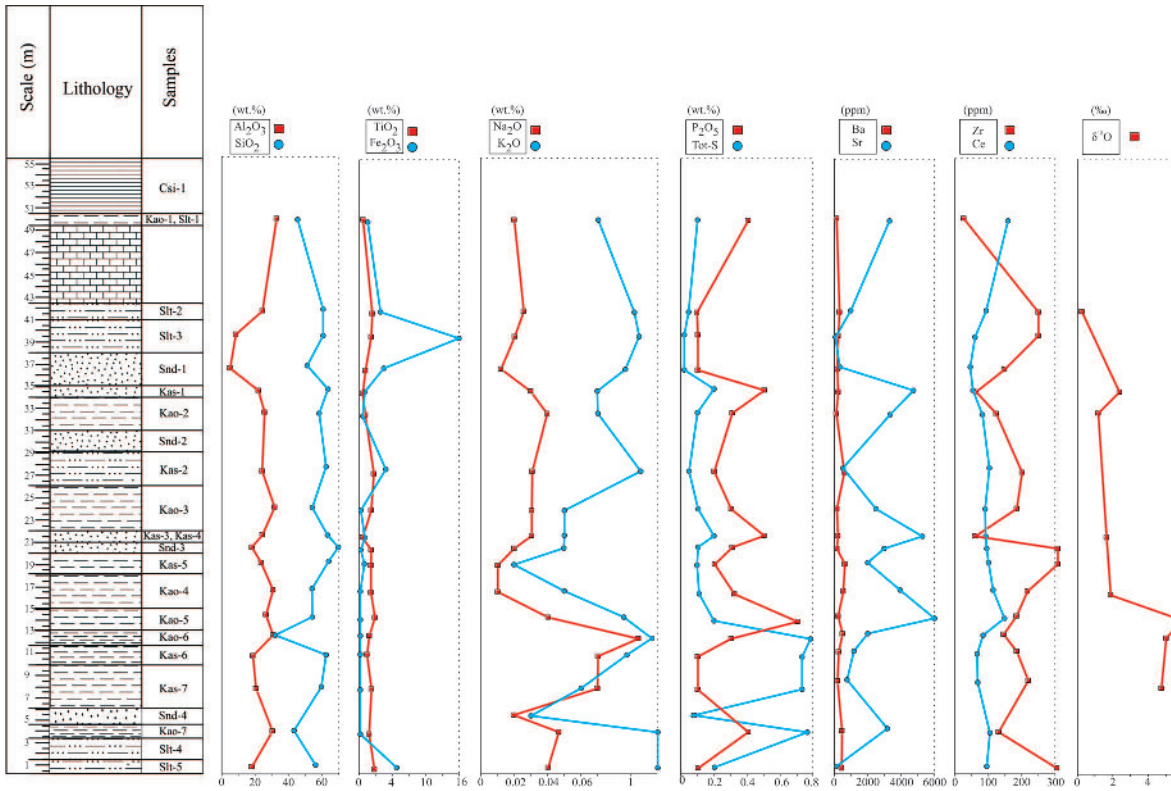

Figure 12. Litholog and chemologs of the Çakmaktepe kaolin deposit in Banaz region.

to 1.37 wt.% in the sedimentary Şile-İstanbul kaolin deposits (Ece *et al.*, 2003), and the Fe_2O_3 concentration decreased slightly in the kaolins. The direct correlation between Fe_2O_3 and K_2O and the inverse correlation between Fe_2O_3 and Al_2O_3 indicated that the Fe_2O_3 contents were generally related to the illite-mica and hematite contents. The Ti, Fe, and K abundances were hosted by argillaceous detrital material and indicated the influx of detritus at the KBST and SLST levels. The total S content varied from 0.14 to 7.28 wt.%, and the P_2O_5 content varied from 0.29 to 0.70 wt.% (Table 2). The abundances of total S, K_2O, and Na_2O were greater in the lower intervals than in the upper levels of the stratigraphic profile (Figure 12). The similarities in the behaviors of the total S, K_2O, and Na_2O abundances in the kaolin intervals and their large total S, K_2O, and Na_2O abundances resulted from the presence of alunite, as indicated by the XRD results of the kaolins (Figure 3; Table 1).

The concentrations of S, Ba, and Sr were enriched in hydrothermally altered rocks. The Cr, Nb, Ti, and *REE* abundances are greater in rocks that have been subjected to supergene alteration (Dill *et al.*, 1997; Marfil *et al.*, 2010). The (Ba+Sr) concentration ranged from 1073.70 ppm to 7637.50 ppm in the kaolinites and from 344.10 ppm to 2432.30 ppm in the KBV rocks. The (Ce+Y+La) concentrations ranged from 105.90 to 281.30 ppm in the kaolinites and from 77.70 to 132.00 ppm in the KBV rocks. The Zr concentrations ranged from 37.90 to 335.00 ppm in the kaolinites and from 128.30 to 186.70 ppm in the KBV rocks. The (Ba+Sr) *vs.* (Ce+Y+La) and Zr *vs.* TiO_2 graphs are presented in Figure 13.

The $\delta^{18}O$ and δD values of the Çakmaktepe kaolins varied from 0.20 to 5.92‰ and from −91.68 to −109.45‰, respectively (Table 4). High $\delta^{18}O$ values (5.92‰ for Kao-5) were detected in the kaolin intervals near the base of the Çakmaktepe deposit. These values decreased from the bottom to the top of the deposit (0.21‰ for Slt-2; Figure 12). The isotopic compositions of the kaolins in this study were compared with the isotopic compositions of clay minerals from the El Salvador porphyry copper deposit in Chile (Sheppard and Gustafson, 1976), the Andacollo Pb-Zn deposit in Neuquen (Dominguez, 1990), the Chubut River valley kaolin deposits in Patagonia (Cravero *et al*, 1991), and the Lastarria kaolins in south-central Chile (Gilg *et al.*, 1999) in a diagram of $\delta^{18}O$ *vs.* δD (Figure 13). The formation temperature for kaolinite was between 92 and 156ºC for the Çakmaktepe kaolins and was 80ºC for the kaolinitic zone in the KBV (Table 4) according to the $\delta^{18}O$ values and the isotopic fractionation factor between kaolinite (α) ($1000 \ln(\alpha) = 2.76*10^6/T^2 - 6.75$) and water, as suggested by Sheppard and Gilg

https://doi.org/10.1346/CCMN.2015.0630401 Published online by Cambridge University Press

Table 3. Major- (wt.%) and trace-element (ppm) data for samples from the Çakmaktepe region.

Sample code Sample type	Csi-1 SL	Kao-1 KAO	Slt-2 KBSL	Slt-3 SLST	Snd-1 SDST	Kas-1 KBST	Kao-2 KAO	Kas-2 KBSL	Kao-3 KAO	Kas-3 KBST	Kas-4 KBST
SiO_2	82.32	47.89	60.96	66.53	51.95	64.78	59.39	62.24	54.21	63.19	66.91
TiO_2	2.02	0.24	0.83	0.75	0.49	0.26	0.40	0.91	0.73	0.22	0.48
Al_2O_3	1.92	31.90	23.99	9.71	6.82	21.58	26.74	23.33	31.25	23.51	21.90
Fe_2O_3	11.17	0.48	1.93	16.20	2.37	0.27	0.20	2.14	0.10	0.32	0.21
MnO	0.03	0.01	0.01	0.12	0.09	0.01	0.01	0.01	0.01	0.01	0.01
MgO	0.08	0.63	0.36	0.66	3.32	0.05	0.04	0.32	0.03	0.09	0.05
CaO	0.36	0.76	0.53	0.30	16.00	0.14	0.09	0.16	0.09	0.22	0.06
Na_2O	0.08	0.02	0.26	0.21	0.13	0.03	0.04	0.33	0.03	0.03	0.05
K_2O	0.18	0.07	1.67	1.54	0.92	0.07	0.07	2.23	0.05	0.05	0.22
P_2O_5	0.10	0.42	0.09	0.10	0.10	0.49	0.29	0.19	0.30	0.54	0.30
Cr_2O_3	0.01	0.05	0.02	0.03	0.02	0.07	0.06	0.05	0.06	0.07	0.08
Total S	0.04	0.16	0.05	0.02	0.02	0.22	0.14	0.05	0.16	0.23	0.20
LOI	1.60	17.00	9.20	3.70	17.60	11.60	12.20	7.90	12.70	11.00	9.30
Total	99.86	99.49	99.82	99.85	99.86	99.37	99.58	99.78	99.58	99.29	99.56
Ba	794.00	105.00	300.00	267.00	181.00	232.00	106.00	540.00	193.00	289.00	172.00
Co	2.30	7.30	2.10	15.00	10.80	0.80	1.40	2.40	0.40	1.40	0.80
Cs	0.90	6.80	6.00	10.50	4.60	0.10	0.10	5.00	0.10	0.10	0.30
Hf	8.50	1.00	6.70	6.90	4.00	2.60	3.70	6.00	5.50	1.40	5.50
Nb	47.40	5.20	16.90	15.40	9.60	4.70	7.90	18.80	15.70	4.50	9.30
Rb	7.60	5.50	72.50	73.40	44.00	1.60	2.00	83.80	0.60	0.50	6.40
Sr	140.10	3491.50	843.60	141.50	314.10	4812.40	3264.00	539.00	2590.80	5266.70	2927.50
Ta	2.40	0.40	1.20	1.10	0.70	0.30	0.60	1.50	1.00	0.30	0.60
Th	7.10	19.40	17.30	9.30	6.10	15.60	13.10	18.00	14.50	10.10	11.90
U	4.80	1.30	2.70	3.30	2.00	1.00	1.90	2.80	3.50	0.90	1.40
V	52.00	108.00	104.00	75.00	49.00	285.00	211.00	88.00	135.00	327.00	95.00
W	7.30	1.00	1.40	1.20	0.80	0.90	1.80	1.90	1.70	0.60	0.90
Zr	301.10	37.90	252.80	264.60	154.50	78.30	137.10	204.00	183.80	61.10	206.70
Y	26.80	5.20	23.80	35.90	18.10	7.30	9.90	27.00	13.70	8.90	8.70
La	19.50	57.90	46.50	33.30	23.70	51.20	38.80	42.80	41.30	54.40	26.50
Ce	39.80	157.40	93.70	64.30	46.20	95.70	74.60	99.20	92.80	95.00	81.50
Pr	5.03	19.29	11.99	8.01	5.89	9.46	8.73	11.27	9.26	11.04	9.85
Nd	20.80	75.30	41.80	30.30	22.30	25.10	26.80	48.90	29.60	49.90	36.70
Sm	3.39	10.26	6.07	6.17	3.82	3.25	5.45	13.05	4.48	12.02	4.37
Eu	0.74	1.80	1.12	1.41	0.82	0.83	0.92	2.99	0.79	2.21	0.63
Gd	3.08	3.38	4.29	6.92	3.43	3.63	2.68	11.77	2.96	6.44	1.96
Tb	0.59	0.28	0.64	1.05	0.54	0.41	0.29	1.21	0.43	0.67	0.29
Dy	3.94	1.13	4.02	5.86	2.84	1.45	1.65	5.52	2.37	2.29	1.60
Ho	0.87	0.18	0.78	1.10	0.57	0.26	0.32	1.03	0.50	0.29	0.34
Er	2.85	0.44	2.29	3.28	1.69	0.66	1.01	3.15	1.61	0.67	0.99
Tm	0.48	0.09	0.41	0.50	0.26	0.10	0.15	0.50	0.25	0.11	0.15
Yb	3.00	0.63	2.49	2.74	1.54	0.63	1.06	3.42	1.82	0.66	1.05
Lu	0.48	0.09	0.37	0.42	0.25	0.09	0.16	0.52	0.28	0.09	0.17
Mo	11.30	0.10	1.40	6.30	1.90	0.80	0.50	0.20	0.10	0.60	0.20
Cu	12.80	19.00	9.20	14.30	9.30	4.80	4.10	12.90	47.00	3.90	13.50
Pb	18.50	1.60	8.10	12.90	8.90	3.70	2.10	1.30	2.70	7.40	1.90
Zn	24.00	5.00	13.00	199.00	47.00	11.00	14.00	3.00	3.00	17.00	1.00
Ni	34.10	14.80	13.70	120.60	50.10	19.90	11.70	5.70	1.90	20.90	1.30
As	36.10	6.20	17.70	84.00	7.00	7.40	0.80	5.90	4.90	16.90	4.70
Sb	1.60	0.10	0.30	0.60	0.10	0.10	0.10	0.60	0.10	0.10	0.10

SLC: silica layer, KAO: kaolin, KBSL: kaolinite-bearing siltstone, SLST: siltstone, SDST: sandstone, KBST: kaolinite-bearing sandstone.

(1996). The formation temperature of kaolinite increased gradually from the bottom to the top of the Çakmaktepe deposit (Table 4). The formation temperature of smectite in the smectitic zone in the KBV was calculated as 87ºC by using the $\delta^{18}O$ values and the isotopic fractionation factor between smectite (α) (1000 ln (α) = $2.58*10^6/T^2 - 4.19$) and water, as suggested by Savin and Lee (1988). The $\delta^{18}O$ value of meteoric water in the formation-temperature calculations was assumed to be −8‰ for the Miocene period (Özyurt and Bayarı, 2005).

https://doi.org/10.1346/CCMN.2015.0630401 Published online by Cambridge University Press

Table 3. Continued.

Sample code Sample type	Snd-3 SNB	Kas-5 KBST	Kao-4 KAO	Kao-5 KAO	Kao-6 KAO	Kas-6 KBST	Kas-7 KBSL	Snd-4 SNB	Kao-7 KAO	Slt-5 SLST
SiO_2	70.28	64.02	54.01	54.84	32.51	63.30	61.24	95.05	41.09	57.71
TiO_2	0.82	0.79	0.88	0.95	0.60	0.46	0.60	1.08	0.62	0.97
Al_2O_3	18.26	23.60	30.27	28.83	31.62	19.27	21.89	2.26	30.77	18.69
Fe_2O_3	0.10	0.33	0.15	0.16	0.15	0.24	0.15	0.23	0.07	5.34
MnO	0.01	0.01	0.01	0.01	0.01	0.01	0.01	0.01	0.01	0.05
MgO	0.05	0.03	0.22	0.10	0.02	0.02	0.02	0.02	0.01	2.77
CaO	1.47	0.11	0.39	0.22	0.12	0.04	0.06	0.03	0.06	2.07
Na_2O	0.02	0.01	0.02	0.04	1.59	0.78	0.69	0.02	0.47	0.46
K_2O	0.05	0.02	0.05	0.09	2.97	0.99	0.64	0.03	2.66	3.48
P_2O_5	0.32	0.20	0.36	0.70	0.33	0.14	0.13	0.07	0.38	0.14
Cr_2O_3	0.06	0.05	0.07	0.09	0.05	0.03	0.04	0.01	0.08	0.04
Total S	0.13	0.11	0.18	0.28	7.28	3.11	2.32	0.07	4.67	0.19
LOI	8.10	10.50	13.00	13.00	29.70	14.50	14.40	1.10	23.30	7.90
Total	99.55	99.63	99.39	98.99	99.65	99.83	99.84	99.92	99.49	99.73
Ba	154.00	600.00	541.00	259.00	421.00	185.00	166.00	18.00	374.00	472.00
Co	1.00	0.80	1.10	1.00	0.30	0.30	0.40	0.70	0.50	154.50
Cs	0.20	0.10	0.20	0.20	0.30	0.10	0.10	0.10	0.10	21.00
Hf	10.00	8.50	6.30	5.60	4.00	4.80	5.80	9.80	4.10	5.80
Nb	15.60	16.00	19.50	21.60	13.30	8.00	11.30	19.00	12.70	21.30
Rb	1.00	0.50	1.70	2.10	57.00	17.20	16.50	0.60	31.60	181.20
Sr	3034.70	2108.20	3886.50	7378.50	2025.30	1069.90	907.70	466.70	3210.10	132.40
Ta	1.20	1.10	1.30	1.60	0.90	0.70	0.80	1.50	0.90	1.40
Th	18.80	15.90	17.30	21.40	14.20	10.70	16.50	7.10	13.10	15.70
U	3.50	2.40	3.20	4.70	2.70	1.40	2.10	4.60	3.00	6.70
V	231.00	127.00	282.00	368.00	193.00	89.00	74.00	55.00	335.00	151.00
W	1.70	1.70	2.60	3.10	1.50	0.80	1.30	1.80	0.60	2.50
Zr	362.30	335.00	214.20	186.70	145.00	178.40	219.80	336.50	134.40	207.00
Y	19.20	19.40	19.10	19.90	12.80	9.50	12.50	17.80	11.20	28.80
La	61.30	56.00	62.10	104.70	49.70	31.00	30.50	25.70	50.20	43.10
Ce	92.70	106.80	129.10	156.70	101.80	66.50	62.90	49.40	110.70	95.90
Pr	9.26	13.87	14.97	15.30	10.95	7.04	7.36	5.20	11.51	10.09
Nd	29.60	54.40	51.90	52.50	38.00	24.20	26.40	19.00	34.80	40.30
Sm	5.09	6.88	6.48	10.65	5.55	3.37	3.29	2.52	2.78	7.67
Eu	0.97	0.90	1.16	2.27	0.89	0.54	0.62	0.44	0.42	1.59
Gd	3.68	3.31	4.06	6.80	2.54	1.77	2.08	2.20	1.69	7.19
Tb	0.55	0.48	0.61	0.80	0.37	0.25	0.31	0.41	0.28	1.02
Dy	3.22	2.78	3.27	3.87	1.97	1.36	1.67	2.63	1.73	5.79
Ho	0.66	0.64	0.69	0.69	0.44	0.33	0.42	0.60	0.40	1.07
Er	1.92	1.91	2.11	2.12	1.40	0.93	1.33	2.03	1.29	3.20
Tm	0.31	0.33	0.34	0.35	0.25	0.15	0.20	0.33	0.21	0.46
Yb	2.07	2.11	2.27	2.20	1.49	1.18	1.44	2.24	1.32	3.09
Lu	0.30	0.33	0.35	0.34	0.24	0.15	0.21	0.35	0.21	0.45
Mo	0.10	1.00	0.10	0.10	0.10	1.00	0.20	0.40	0.30	1.30
Cu	1.80	2.60	4.80	5.40	1.70	3.10	2.10	1.80	14.10	40.20
Pb	13.60	8.40	5.70	14.60	4.20	1.40	1.00	1.10	3.00	18.50
Zn	4.00	49.00	12.00	13.00	4.00	2.00	2.00	4.00	2.00	139.00
Ni	1.50	11.30	14.30	11.80	1.70	1.20	1.20	2.00	3.10	510.00
As	4.90	3.50	6.00	3.80	12.90	11.10	11.40	1.70	11.80	17.90
Sb	0.10	0.10	0.10	0.10	0.10	0.10	0.10	0.10	0.10	0.60

SNB: sand bed, KBST: kaolinite-bearing sandstone, KAO: kaolin, KBSL: kaolinite-bearing siltstone, SLST: siltstone.

DISCUSSION

Kaolin deposits are formed from two different geological processes: (1) hydrothermal and residual alteration of crystalline rocks (primary kaolins); and (2) alteration, erosion, transportation, and deposition of kaolinite elsewhere (secondary kaolins). Hydrothermal and weathering processes influence the occurrence of kaolinites before transportation in secondary deposits (Murray, 1988; Kitagawa and Köster, 1991; Montes *et al.*, 2002; Ece *et al.*, 2003; Dominguez *et al.*, 2008; Dill, 2010; Marfil *et al.*, 2010). The geology and geometry of

https://doi.org/10.1346/CCMN.2015.0630401 Published online by Cambridge University Press

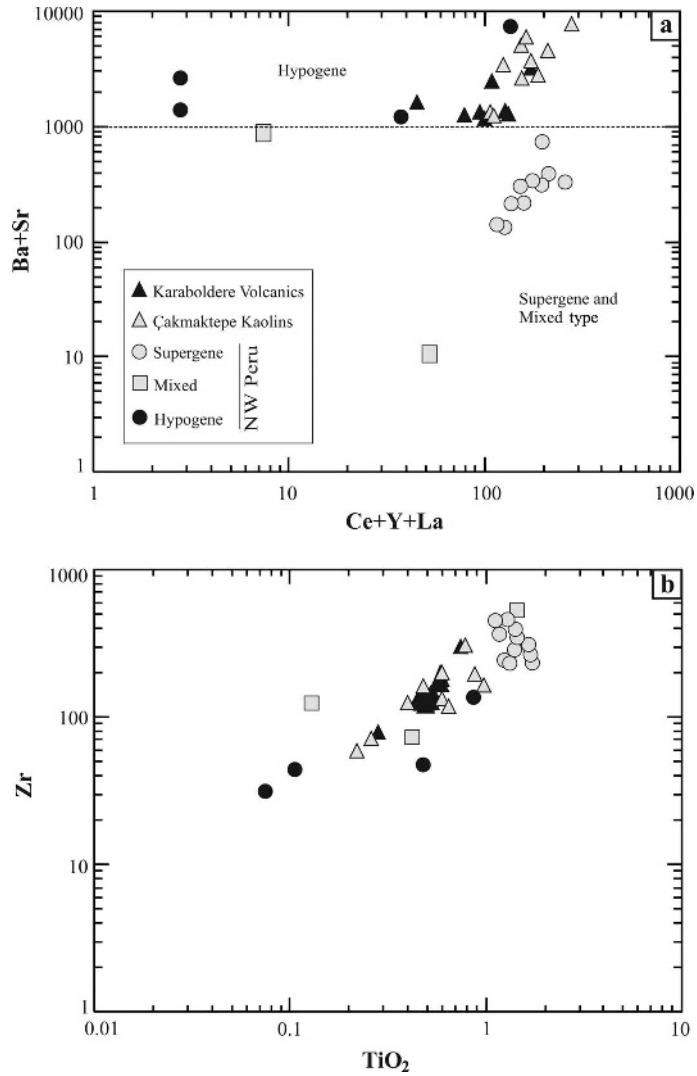

Figure 13. Data plot of Karaboldere volcanics and Çakmaktepe kaolins. Data for supergene, mixed, and hypogene kaolins are from Dill *et al*. (1997). (a) Binary diagram discriminating between hypogene and supergene genesis of altered volcanics and Çakmaktepe kaolins with the hypogene–supergene (dotted) line of Dominguez *et al*. (2008); and (b) relation between total TiO_2 and Zr contents in the Karaboldere volcanics and the Çakmaktepe kaolins.

Table 4. $\delta^{18}O$, δD, and formation-temperature values of samples from the Çakmaktepe region.

Sample code	Sample type	$\delta^{18}O$ (‰)	δD (‰)	Formation temperature (ºC)
Slt-2	KBSL	0.21	−109.45	156
Kas-1	KBST	2.41	−104.1	139
Kao-2	KAO	1.18	−109.37	142
Kas-3	KBST	1.69	−102.32	136
Kao-4	KAO	1.85	−91.68	134
Kao-5	KAO	5.92	−105.51	92
Kao-6	KAO	4.98	−104.15	100
Kas-7	KBSL	4.75	−67.79	102
San-2	TAN	7.26	−79.82	80
San-9	TAN	6.52	−111.13	87

Note: KBSL: Kaolinite-bearing siltstone, KBST: Kaolinite-bearing sandstone, SLST: Siltstone, SDST: Sandstone, SNB: Sand bed, and TAN: Trachyandesite.

https://doi.org/10.1346/CCMN.2015.0630401 Published online by Cambridge University Press

the deposit, the presence and distribution of certain mineral phases such as alunite and Fe-Ti oxide, the major and trace elements, and the stable isotope compositions of kaolinite may provide information regarding the origin of kaolinization (Kelepertis and Esson, 1987; Boulvais *et al.*, 2000; Siddiqui and Ahmed, 2008). Unlike the primary kaolin hypothesis of Erkoyun and Kadir (2011), the present authors suggest that Çakmaktepe kaolins are secondary-type kaolins. The following data support our argument: (1) the stratified shape of the deposit; (2) the intercalation of kaolin intervals with sedimentary units, such as limestone, sandstone, siltstone, and sand layers (3); sedimentary structures in the kaolin and KBS levels; (4) similarities in the mineralogical and geochemical compositions of the alteration zones in the KBV and Çakmaktepe kaolins; (5) decreasing $\delta^{18}O$ values from the bottom to the top of the deposit; and (6) the microscopic properties of the Çakmaktepe kaolins.

The argillic alteration zones in KBV have similar mineralogical composition to Çakmaktepe kaolins and contain kaolinite, smectite, cristobalite/opal-CT, alunite, and hematite. The zonation of the minerals from the outer zone to the inner zone in the argillic alteration serves as the most important indicator of the hydrothermal origin of the kaolins in the KBV. Such lateral zonation of clay minerals has been observed in many hydrothermally altered magmatic rocks due to the irregular distribution of the discontinuous horizons with different permeabilities and porosities (Karakaya *et al.*, 2001; Kadir and Akbulut, 2009; Kadir and Erkoyun, 2012). Physicochemical and environmental conditions controlled the formation of kaolinite, alunite, and smectite in these kaolins (Sayın, 2007; Kadir *et al.*, 2011; Ece *et al.*, 2013). Alunite is a characteristic mineral of hydrothermal kaolins formed under acidic conditions from the reaction of SO_4^{2-}-bearing solutions with volcanic glass and feldspar in volcanic rocks. When the pH of the solution is 4–5, kaolinite precipitates with or without alunite (Karakaya *et al.*, 2001). Smectite occurs under alkaline conditions with high cation/H^+ ratios and is converted to kaolinite as the pH and cation/H^+ ratios decrease in various environments (Christidis and Marcopulos, 1995). According to Pevear *et al.* (1980) and Senkayi *et al.* (1987), smectite and cristobalite are the initial alteration products of volcanic materials, and kaolinite represents an advanced stage of alteration. Fe, Mg, Ca, Na, and K were leached extensively, and Al was enriched during kaolinization (Kelepertsis and Esson, 1987). The loss of alkalis and Mg enrichment are required for the formation of smectite when the pore fluids have low salinity and alkalinity (Christidis, 1998; Yıldız and Kuşcu, 2004). The depletion of the alkali elements, Fe, Mg, Zr, *LREE* relative to the fresh/unaltered volcanic rocks; the enrichment of Hf, Nb, Ta, and *HREE*; and the presence of negative Eu anomalies are closely related to the alterations of K-feldspar, plagioclase, hornblende, and volcanic glass in altered volcanics as shown in Figures 10 and 11.

The trace-element abundances and the ratios of Zr to TiO_2 and (Ba+Sr) to (Ce+Y+La) are useful tools for distinguishing between hypogene and supergene kaolinization in source areas of sedimentary kaolins. The *REE* and HFS element concentrations, such as Zr and Ti, in sedimentary clays may reflect the compositions of their protoliths. These elements show relatively low mobility during weathering, transport, diagenesis, and metamorphism (Taylor and McLennan, 1985; Saleemi and Ahmed, 2000). Kaolin deposits of hypogene origin have high Ba and Sr contents because the Ba and Sr are primarily bound in barite, which typically occurs in hypogene kaolin deposits (Dill *et al.*, 2008; Marfil *et al.*, 2010; Grecco *et al.*, 2012). The Ba and SO_3 contents indicate the presence of barite, which was verified in the Çakmaktepe kaolins (Figure 8d). Barite, however, was not detected in XRD studies due to its lower concentration in the Çakmaktepe kaolins. In contrast, Ce, Y, and La are enriched during supergene kaolinization (Dill *et al.*, 1997; Cravero *et al.*, 2001; Marfil *et al.*, 2010). The altered volcanics, Çakmaktepe kaolins, and hypogene kaolin samples from northwestern Peru plotted in the hypogene area (Figure 13a). Under near-atmospheric conditions, Zr is immobile and serves as a good indicator of the degree of weathering of the parent rock. During hypogene or supergene alteration, Ti may be released from primary minerals in the parent rock and precipitate as anatase or rutile in the nanocrystalline form (Schroeder and Shiflet, 2000). The high Zr and Ti contents in the kaolin samples demonstrate the superficial environment of formation (Dill *et al.*, 1997), and the Fe_2O_3 + TiO_2 contents of the hypogene kaolinites have been shown to be <1% (Marfil *et al.*, 2010). In the Zr *vs.* TiO_2 diagram (Figure 13b), the Zr and TiO_2 contents of the Çakmaktepe kaolins and altered volcanics are comparable and show trends similar to those of hypogene kaolins from northwestern Peru.

The isotopic composition of kaolinite relates to the conditions (*i.e.* supergene, sedimentary, and hydrothermal) during alteration because it was not affected by deposition (Savin and Lee, 1988). Thus, the oxygen isotopic composition ranges from +19 to +23‰ in kaolinites of sedimentary origin, from +15 to +19‰ in kaolinites of residual origin, and from +15 to −9.2‰ in kaolinites of hydrothermal origin (Murray and Janssen, 1984; Sheppard and Gilg, 1996; Marfil *et al.*, 2005). The oxygen isotope results from the Çakmaktepe kaolins are consistent with a hydrothermal origin. Sheppard *et al.* (1969), Marumo *et al.* (1982), and Sheppard and Gilg (1996) discriminated between supergene and hypogene kaolins using stable oxygen and hydrogen isotopes. Çakmaktepe kaolins, Karaboldere volcanics, kaolinites from El Salvador and Andacollo, and Lastarria kaolins are scattered to the left of the hypogene-supergene line

https://doi.org/10.1346/CCMN.2015.0630401 Published online by Cambridge University Press

(Figure 14), indicating that the kaolins in the Çakmaktepe deposits are of hypogene origin. Low δD values result from mixing meteoric waters during magmatic events (Taylor, 1992; Hedenquist, *et al.*, 1998). The distribution of the Çakmaktepe kaolinites parallel to the kaolinite line in Figure 14 indicates that the kaolinite crystals formed at different temperatures and under different water compositions (Meunier, 2005). The calculated formation temperatures of the Çakmaktepe kaolinites were between 92 and 156ºC when using their $\delta^{18}O$ values. These data were comparable with those from the kaolinitic zone in the KBV (80ºC), the hydrothermally altered kaolinite deposits in western Anatolia (Kadir *et al.*, 2011; Kadir and Erkoyun, 2012), and the reservoir temperatures (81−130ºC) of the thermal waters in the Hamamboğazı region, which is located <20 km southwest of the study area (Davraz, 2008). The trend of the formation temperature values of the kaolinites from the base to the top of the Çakmaktepe deposit revealed that the kaolins were not derived from the *in situ* alteration in the Çakmaktepe region and that the hydrothermal alteration products of KBV were deposited in the Çakmaktepe region (Table 4; Figure 12). Meunier (2005) suggested that the formation temperatures of clay minerals in hydrothermal systems show an increase which is more or less consistent with depth. The mineralogical, trace-element, and isotope data suggested that the Çakmaktepe kaolins were derived from argillaceous alteration zones in volcanic rocks of the Kozören district. The textural features and distributions of kaolinite crystals observed in the SEM images provide information regarding the origins of the deposits (Keller, 1976, 1989; Bauluz *et al.*, 2008). The dissolution-decomposition and replacement-crystallization mechanisms representing the alteration of parent minerals are major textural features of primary kaolins (weathering, diagenesis, and hydrothermal) (Keller, 1976; Kitagawa and Köster, 1991; Ekosse, 2000; Bauluz *et al.*, 2008; Dominguez *et al.*, 2008; Kadir *et al.*, 2011). Kaolinites in secondary deposits, however, occur within more tightly packed aggregates and exhibit irregular arrangements and grain-size fractionation (Henning and Störr, 1986; Keller, 1977). The deficiency of dissolution-decomposition and replacement-crystallization mechanisms, which reflect *in situ* alteration; the irregular edge-to-face arrangement of the kaolinite crystals; a few broken kaolinite crystals; low sphericity, very angular, and poorly sorted quartz crystals; and the variations in the grain-size of the kaolinite crystals in different kaolin layers, all indicate that transportation and sedimentation processes occurred after hydrothermal alteration.

The alternations in the SNB and KBST levels and the graded and cross-bedding structures in the kaolins reflect sedimentary processes, such as fluctuations in source type, rainfall, temperature, topography, and depositional-energy. Most of the clay was carried in suspension in

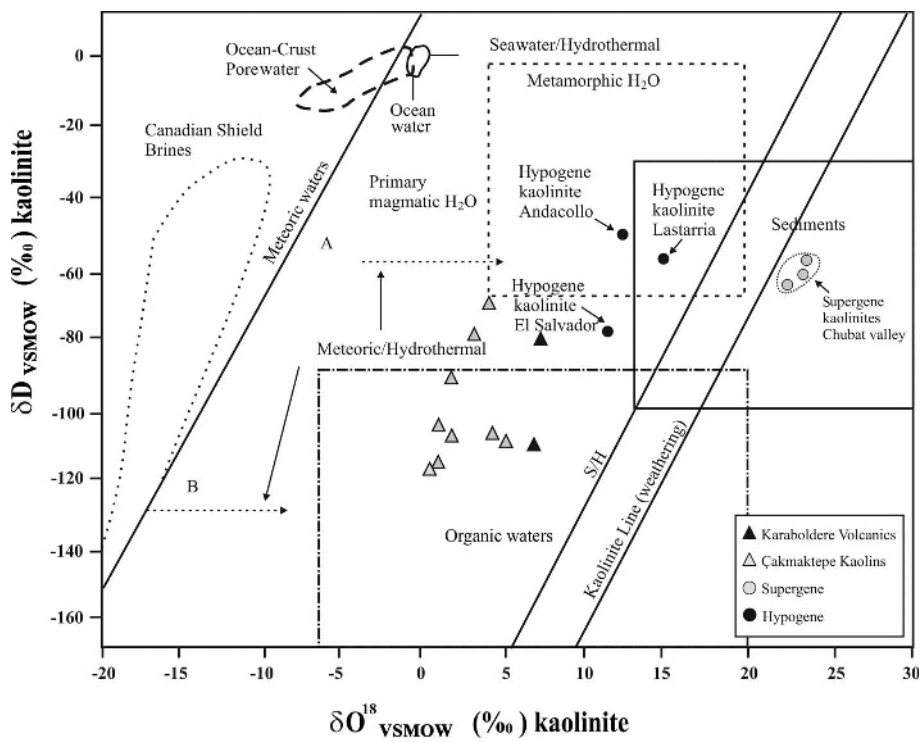

Figure 14. Cross plot of oxygen and hydrogen isotope compositions of samples from the Çakmaktepe and Kozören districts with the hypogene-supergene (S/H) line of Sheppard *et al* (1996) and the kaolinite line modified by Sheppard and Gilg (1996) after Savin and Epstein (1970).

https://doi.org/10.1346/CCMN.2015.0630401 Published online by Cambridge University Press

the river systems. The flow velocity and relief affected the sizes of the suspended materials (Weaver, 1989; Hillier, 1995). A slow flow velocity was associated with surfaces with low relief. Fine-grained materials, such as kaolinites, were transported in these environments. Turbulent flow regimes in high-relief areas generally result in the transport of coarse-grained sand and silt. The presence of detrital minerals, *e.g.* quartz, feldspar, and micas, in the high-relief regions of the study area, indicate that physical weathering occurred. The sand layers in the Çakmaktepe deposit resulted from the alteration products of granitic-rock outcrops on the NW side of the study area. Similar sandy sediments were observed in the kaolinite deposit of Şile (northern İstanbul), and Ece *et al.* (2003) revealed that sand intervals within the clay deposit reflected river sedimentation. The alternation of kaolin inervals with sand layers within the Çakmaktepe deposit and the increasing kaolinite abundances in the kaolin layers from the bottom to the top of the section (from Kas-7 to Kao-4) suggested seasonal variations in rainfall. Kennedy (1964) suggested that the amount of clay in the suspended load was not only a function of flow velocity, but also of the degree of alteration, amount of runoff, and position in the river channel. Kennedy (1964) also reported an increase in the suspended clay content in Georgia (U.S.A.) rivers after intensive rainfalls. According to Nichols (2009b), load casts, cusps, tool marks, and current ripples between the kaolin and the KBST and SNB levels indicated turbulent flow. Potter *et al.* (2005) suggested that these sedimentary structures represented the sinking of fine sand and silt into less dense, soft, and water-saturated clay-rich levels. Clastic sediments (such as clay, silt, and sand), limestone intervals, erosional surfaces (Figure 4b), and current ripples (Figure 4e) at the contacts of terrigenous clastic sediments with kaolins in the Çakmaktepe kaolin deposits indicated that deposition occurred in different regions of the lake. Coarse clastic sediments were deposited in shoreline and shallow-lake environments, and carbonates settled in the deeper portion of the lake.

The silica level in the uppermost part of the Çakmaktepe deposit was formed by the deposition of dissolved silica under neutral and basic conditions in a shallow-lake environment depending on the pH, temperature, and silica concentrations as chert. Silicification is associated with hydrothermal processes that serve as a possible source of dissolved silica in volcanic areas (Hesse, 1989). Opal-A is a hydrated amorphous silica phase and occurs in the early stages of conversion from opal-A to opal-CT during diagenesis. Next, dissolution-precipitation reactions resulted in the transformation of Opal-CT to microcrystalline quartz (Knauth, 1994; Marin-Carbonne *et al*., 2014). The rate of the silica transformation is higher in carbonates than in clays. Silica either precipitates residually at selected sites due to a lack of flow pathways or accumulates within the lake environment after being carried by rivers (Miretzky *et al*., 2001; Rodgers *et al*., 2004). Excessive alkali and Mg concentrations in the lakes contribute to the conversion of opal-A to α-quartz. Hence, opal-CT does not occur in lakes (Williams and Crerar, 1985). The existence of microcrystalline quartz and the absence of opal-CT from XRD and SEM determinations at the silica level of Çakmaktepe deposits indicate the silica level deposited in the alkali-lake environment.

CONCLUSIONS

New data from mature production faces in the Çakmaktepe mine and from the volcanic alteration zones in the surrounding areas support the suggestion that the Çakmaktepe kaolins were formed by hydrothermal alteration of the Karaboldere volcanics (KBV). Kaolinized material was then eroded and transported to the Çakmaktepe region and deposited with other Yeniköy Formation components in a lacustrine environment. The lateral zonation of alteration minerals, the presence of alunite with kaolinite, and the high degree of crystallinity of the kaolinites suggest the effects of hydrothermal fluids on Çakmaktepe kaolins and KBV. The combination of trace-element and $\delta^{18}O$- and δD-isotope data indicated that the Çakmaktepe kaolin deposits were of hypogene origin and were formed during alteration of the KBV by hydrothermal fluids. These hydrothermal fluids were formed when the meteoric-magmatic waters were mixed at between 92 and 156ºC, and these data correspond with the kaolinitic zone in the KBV (80ºC) and the reservoir temperatures (81–130ºC) of the thermal waters in the Hamamboğazı region. The stratified geometry of the kaolin deposit, intercalation of the kaolin intervals with the terrigenous sediments and limestone, sedimentary structures between different kaolin layers, microscopic properties of the kaolinite and quartz grains in the Çakmaktepe kaolins, and higher formation-temperature values of the kaolinites from the bottom to the top of the Çakmaktepe deposit can only be explained by transportation and deposition processes after hydrothermal alteration.

ACKNOWLEDGMENTS

The present study was subsidized by the 'Coordinatorship of Scientific Research Projects of Afyon Kocatepe University', project number 07.MUH.01. The authors are grateful to the Uşak Ceramic Company for technical support to complete field and laboratory works. They also thank Prof. Dr. Harald G. Dill, Prof. Dr. Ö. Işık Ece, Prof. Dr. George E. Christidis, and Prof. Dr. Muazzez Çelik Karakaya for their constructive reviews which helped to improve the manuscript.

REFERENCES

Arslan, M., Kadir, S., Abdioğlu, E., and Kolaylı, H. (2006) Origin and formation of kaolin minerals in saprolite of Tertiary alkaline volcanic rocks, Eastern Pontides, NE Turkey. *Clay Minerals*, **41**, 597–617.

Aydoğan, M.S., Çoban, H., Bozcu, M., and Akıncı, Ö.T. (2006) Geochemical and mantle-like isotopic (Nd, Sr) composition of the Baklan Granite from the Muratdağı Region (Banaz, Uşak), western Turkey: Implications for input of juvenile magmas in the source domains of western Anatolia Eocene Miocene granites. *Journal of Asian Earth Sciences*, **33**, 155–176.

Başaran, C. (2009) Hallaçlar (Banaz-Uşak) kaolen yataklarının jeolojik, mineralojik ve jeokimyasal özelliklerinin araştırılması. MSc thesis, Afyon Kocatepe Universitesi, 139 pp., Afyonkarahisar, Turkey (in Turkish, unpublished).

Bauluz, B., Mayayo, M.J., Yuste, A., and Gonzalaez Lopez, J.M. (2008) Genesis of kaolinite from Albian sedimentary deposits of the Iberian Range (NE Spain): analysis by XRD, SEM and TEM. *Clay Minerals*, **43**, 459–475.

Boulvais, P., Vallet, J.M., Esteoule-Choux, J., Fourcade, S., and Martineau, F. (2000) Origin of kaolinization in Brittany (NW France) with emphasis on deposits over granite: stable isotopes (O, H) constraints. *Chemical Geology*, **168**, 211–223.

Bozkurt, E. and Mittwede, S.K. (2005) Introduction: evolution of Neogene extensional tectonics of western Turkey. *Geodinamica Acta*, **18**, 153–165.

Bozkurt Çiftçi, N. and Bozkurt, E. (2009) Pattern of normal faulting in the Gediz Graben, SW Turkey. *Tectonophysics*, **473**, 234–260.

Bristow, C.M. (1987) World kaolins: Genesis, exploitation and application. *Industrial Minerals*, **July**, 45–59.

Brooks, R.A. and Ferrell, R.E., Jr. (1970) The lateral distribution of clay minerals in Lake Pontchartrain and Maurepas, Louisiana. *Journal of Sedimentary Petrology*, **40**, 855–863.

Brown, G. (1972) Montmorillonites. Pp. 143–206 in: *X-ray Identification and Crystal Structures of Clay Minerals*. Mineral Society, London.

Brown, G. and Brindley, GW. (1980) X-ray diffraction procedures for clay mineral identification. Pp. 495 in: *Crystal Structure of Clay Minerals and their X-ray Identification* (G. W. Brindley and G. Brown, editors). Monograph **5**, Mineralogical Society, London.

Christidis, G.E. (1998) Comparative study of the mobility of major and trace elements during alteration of an andesite and a rhyolite to bentonite, in the islands of Milos and Kimolos, Aegean, Greece. *Clays and Clay Minerals*, **46**, 379–399.

Christidis, G. and Markopoulos, T. (1995) Mechanisms of formation of kaolinite and halloysite in the bentonite deposits of Milos Island, Greece. *Chemie der Erde*, **55**, 315–329.

Christidis, G., Scott, P.W., and Marcopoulas, T. (1995) Origin of the bentonite deposits of Eastern Milos and Kimolos, Greece, geology, geological, mineralogical and geochemical evidence. *Clays and Clay Minerals*, **43**, 63–77.

Chung, F.H. (1974) Quantitative interpretation of X-ray diffraction patterns of mixtures. II. Adiabatic principle of X-ray diffraction analysis of mixtures. *Journal of Applied Crystallography*, **7**, 526–531.

Churchman, G.J., Whitton, J.S., Claridge, G.G., and Theng, B.K.G. (1984) Intercalation method using formamide for differentiating halloysite from kaolinite. *Clays and Clay Minerals*, **32**, 241–248.

Corfu, F. and Davis, D.W. (1991) Comment on ''Archaean hydrothermal zircon in the Abitibi greenstone belt: constraints on the timing of gold mineralisation'' by J.C. Claoue-Long, R.W. King and R. Kerrich. *Earth and Planetary Science Letters*, **104**, 545–552.

Cravero, F., Domínquez, E., and Murray, H.H. (1991) Valores $\delta^{18}O$ vs. δD en caolinitas indicatores de un clima templadohumedo para el Jurasico superior-Cretcio inferior de la Patagonia. *Revista de la Asociacion Geologica Argentina*, **46**, 20–25.

Cravero, F., Domínquez, E., and Iglesias, C. (2001) Genesis and applications of the Cerro Rubio kaolin deposit, Patagonia (Argentina). *Applied Clay Science*, **18**, 157–172.

Çelik, M., Karakaya, N., and Temel, A. (1999) Occurrences of clay minerals in hydrothermally altered volcanic rocks, Eastern Pontides, Turkey. *Clays and Clay Minerals*, **47**, 708–717.

Davraz, A. (2008) Hydrogeochemical and hydrogeological investigations of thermal waters in the Usak area. *Environmental Geology*, **54**, 615–628.

Dill, H.G. (2010) The "chessboard" classification scheme of mineral deposits: Mineralogy and geology from aluminum to zirconium. *Earth-Science Reviews*, **100**, 1–420.

Dill, H.G., Bosse, H.R., Henning, K.H., Fricke, A., and Ahrend, H. (1997) Mineralogical and chemical variations in hypogene and supergene kaolin deposits in a mobile fold belt in the Central Andes of NW Peru. *Mineralium Deposita*, **32**, 149–163.

Dill, H.G., Kus, J., Dohrmann, R., and Tsoy, Y. (2008) Supergene and hypogene alteration in the dual-use kaolin-bearing coal deposit Angren, SE Uzbekistan. *International Journal of Coal Geology*, **75**, 225–240.

Dominguez, E. (1990) $\delta^{18}O$ ‰, $\delta^{34}S$ ‰, δD ‰ en pirita caolinita como indicators de procesos hidrotemales magmaticos en Andacollo, Neuquen. (nota breve). *Revista de la Asociacion Geologica Argentina*, **45**, 403–406.

Dominguez, E., Iglesias, C., and Dondi, M. (2008) The geology and mineralogy of a range of kaolins from the Santa Cruz and Chubut Provinces, Patagonia (Argentina). *Applied Clay Science*, **40**, 124–142.

Dominquez, E.A., Iglesias, C., Dondi, M., and Murray, H.H. (2010) Genesis of the La Espingarda kaolin deposit in Patagonia. *Applied Clay Science*, **47**, 290–302.

DPT (2001) State Planning Organization of Turkey, 8th Five-Year Development Plan, Mining Special Expert Comission Report, Volume 1, Industrial Minerals Sub-Comission, Ceramic Clays-Kaolin-Pyrophyllite-Wollastonite-Talc Group, 224 pp., Ankara (in Turkish).

Dunham, R.J. (1962) Classification of carbonate rocks according to depositional texture. Pp. 108–121 in: *Classification of Carbonate Rocks* (W.E. Ham, editor). Memoir 1, American Association of Petroleum Geologists, Tulsa, Oklahoma, USA.

Ece, O.I. and Nakagawa, Z.E. (2003) Alteration of volcanic rocks and genesis of kaolin deposits in the Sile Region, northern Istanbul, Turkey. Part II: Differential mobility of elements. *Clay Minerals*, **38**, 529–550.

Ece, O.I. and Schroeder, P.A. (2007) Clay mineralogy and chemistry of halloysite and alunite deposits in the Turplu area, Balıkesir, Turkey. *Clays and Clay Minerals*, **55**, 18–35.

Ece, O.I., Nakagawa, Z.E., and Schroeder, P.A. (2003) Alteration of volcanic rocks and genesis of kaolin deposits in the Sile Region, northern Istanbul, Turkey. I: Clay mineralogy. *Clays and Clay Minerals*, **51**, 675–688.

Ece, O.I., Schroeder, P.A., Smilley, M., and Wampler, M. (2008) Acid-sulphate alteration of volcanics rocks and genesis of halloysite and alunite deposits in the Biga Peninsula, NW Turkey. *Clay Minerals*, **43**, 281–315.

Ece, O.I., Ekinci, B., Schroeder, P.A., Crowe, D., and Esenli, F. (2013) Origin of the Düvertepe kaolin-alunite deposits in Simav Graben, Turkey: timing and styles of hydrothermal mineralization. *Journal of Volcanology and Geothermal Research*, **255**, 57–78.

Ekosse, G. (2000) The Makoro kaolin deposit, southeastern Botswana: its genesis and possible industrial applications. *Applied Clay Science*, **16**, 301–320.

Ercan, T., Dinçel, A., Metin, S., Türkecan, A., and Günay, E. (1978) Uşak yöresindeki Neojen havzaların jeolojisi. *Türkiye Jeoloji Bülteni*, **21**, 97–106 (in Turkish).

Ercan, T., Dinçel, A., and Günay, E. (1979) Uşak volkanitlerinin petrolojisi ve plaka tektoniği açısından Ege Bölgesindeki yeri. *Türkiye Jeoloji Bülteni*, **22**, 185–198, (in Turkish).

Ercan, T., Satır, M., Sevin, D., and Türkecan, A. (1996) Batı Anadolu'daki Tersiyer ve Kuvaterner yaslı Volkanik Kayaçlarda yeni yapılan radyometrik yas ölçümlerinin yorumu. *Maden Tetkik ve Arama Dergisi*, **119**, 103–112 (in Turkish).

Erkoyun, H. and Kadir, S. (2011) Mineralogy, micromorphology, geochemistry and genesis of hydrothermal kaolinite deposit and altered Miocene host volcanites in the Hallaçlar area, Uşak, western Turkey. *Clay Minerals*, **46**, 421–448.

Floyd, P.A. and Winchester, J.A. (1978) Identification and discrimination of altered and metamorphosed volcanic rocks using immobile elements. *Chemical Geology*, **21**, 291–306.

Fujii, N., Kayabalı, İ., and Saka, A.H. (1995) Data book of ceramic raw materials of selected areas in Turkey. Monograph Series No. **1**, General Directorate of Mineral Research and Exploration, 144 pp., Ankara.

Galan, E., Mattias, P.P., and Galvan, J. (1977) Correlation about kaolin genesis and age of some Spanish kaolinites. Proceedings of the 8th International Symposium and Meeting on Alunite (E. Galen, editor). Ministerio de Industria y Energia, Madrid, K-8, 8 pp.

Genna, D., Gaboury, D., and Roy, G. (2014) Evolution of a volcanogenic hydrothermal system recorded by the behavior of LREE and Eu: Case study of the Key Tuffite at Bracemac–McLeod deposits, Matagami, Canada. *Ore Geology Reviews*, **63**, 160–177.

Gilg, H.A., Hülmeyer, S., Miller, H., and Sheppard, S.M.F. (1999) Supergene origin of the Lastarria kaolin deposit, South-Central Chile, and paleoclimatic implications. *Clays and Clay Minerals*, **47**, 201–211.

Grecco, L.E., Marfil, S.A., and Maiza, P.J. (2012) Mineralogy and geochemistry of hydrothermal kaolins from the Adelita mine, Patagonia (Argentina); relation to other mineralization in the area. *Clay Minerals*, **47**, 131–146.

Hedenquist, J.W., Arrıbas, A., and Reynolds, T.J. (1998) Evolution of an intrusion-centered hydrothermal system: Far southeast-Lepanto porphyry and epithermal Cu-Au deposit, Philippines. *Economic Geology*, **93**, 373–404.

Hedenquist, J., Arribas, R., and González-Urien, E. (2000) Exploration for epithermal gold deposits. Pp. 245–277 in: *Gold in 2000* (S. Hagemann, P.E. Brown, editors). Reviews in Economic Geology, **13**, Society for Economic Geology, Golden, Colorado, USA.

Helvacı, C. (1986) Stratigraphic and structural evolution of the Emet Borate Deposits, Western Anatolia, Turkey. Dokuz Eylül University, İzmir, Turkey, Research Paper MM/JEO-86-8.

Henning, K.H. and Störr, H. (1986) Electron micrographs (TEM, SEM) of clays and clay minerals. Akademia-Verlag, Berlin, 350 pp.

Hesse, R. (1989) Silica diagenesis: Origin of inorganic and replacement cherts. *Earth-Science Reviews*, **26**, 253–284.

Hillier, S. (1995) Erosion, sedimentation and sedimentary origin of clays. Pp. 162–219 in: *Origin and Mineralogy of Clays*: *Clays and Environment* (B. Velde, editor). Springer, Berlin.

Honty, M. Clauer, N., and Šucha, V. (2008) Rare-earth elemental systematic of mixed-layered illite-smectite from sedimentary and hydrothermal environments of the western Carpathians (Slovakia). *Chemical Geology*, **249**, 167–190.

Hurst, V.J. and Pickering, S.M. (1997) Origin and classification of coastal-plain kaolins, southeastern USA, and the role of groundwater and microbial action. *Clays and Clay Minerals*, **45**, 274–285.

Jiang, S.Y. (2000) Controls on the mobility of high field strength elements (HFSE), U, and Th in an ancient submarine hydrothermal system of the Proterozoic Sullivan Pb–Zn–Ag deposit, British Columbia, Canada. *Geochemical Journal*, **34**, 341–348.

Jiang, N., Sun, S., Chu, X., Mizuta, T., and Ishiyama, D. (2003) Mobilization and enrichment of high-field strength elements during late- and post-magmatic processes in the Shuiquangou syenitic complex, Northern China. *Chemical Geology*, **200**, 117–128.

Jiang, S.Y., Wang, R.C., Xu, X.S., and Zhao, K.D. (2005) Mobility of high field strength elements (HFSE) in magmatic-, metamorphic-, and submarine hydrothermal systems. *Physics and Chemistry of the Earth*, **30**, 1020–1029.

Kadir, S. and Akbulut, A. (2009) Mineralogy, geochemistry and genesis of the Taşoluk kaolinite deposits in Pre-Early Cambrian metamorphites and Neogene volcanites of Afyonkarahisar, Turkey. *Clay Minerals*, **44**, 89–112.

Kadir, S. and Kart, F. (2009) The occurrence and origin of the Söğüt kaolinite deposits in the Paleozoic Sarıcakaya granite-granodiorite complexes and overlying Neogene sediments (Bilecik, Northwestern Turkey). *Clays and Clay Minerals*, **57**, 311–329.

Kadir, S., Erman, H., and Erkoyun, H. (2011) Mineralogical and geochemical characteristics and genesis of hydrothermal kaolinite deposits within Neogene volcanites, Kütahya (western Anatolia), Turkey. *Clays and Clay Minerals*, **59**, 250–276.

Kadir, S. and Erkoyun, H. (2012) Genesis of hydrothermal Karaçayır kaolinite deposits in Miocene volcanics and Paleozoic metamorphic rocks of the Uşak-Güre Basin, western Turkey. *Turkish Journal of Earth Sciences*, **22**, 444–468.

Karakaya, M., Karakaya, N., and Temel, A. (2001) Kaolin occurrences in Erenler Dağı volcanics, Southwest Konya Province, Turkey. *International Geology Review*, **43/8**, 711–722.

Karakaya, N. (2009) REE and HFS element behaviour in the alteration facies of the Erenler Dağı volcanics (Konya, Turkey) and kaolinite occurrence. *Journal of Geochemical Exploration*, **101**, 185–208.

Karakaya, M., Karakaya, N., Küpeli, Ş., and Yavuz, F. (2012) Mineralogy and geochemical behavior of trace elements of hydrothermal alteration types in volcanogenic massive sulfide deposits, NE Turkey. *Ore Geology Reviews*, **48**, 197–224.

Karaoğlu, Ö., Helvacı, C., and Ersoy, Y. (2010) Petrogenesis and 40 Ar/ 39 Ar geochronology of the volcanic rocks of the Uşak-Güre basin, western Türkiye. *Lithos*, **119**, 193–210.

Kelepertsis, A.E. and Esson, J. (1987) Major and trace element mobility in altered volcanic rocks near Stypsi, Lesbos, Greece and genesis of kaolin deposit. *Applied Clay Science*, **2**, 11–28.

Keller, W.D. (1976) Scanning electron micrographs of kaolins collected from diverse environments of origin – I. *Clays and Clay Minerals*, **24**, 107–113.

Keller, W.D. (1977) Scanning electron micrographs of kaolins collected from diverse environments of origin – IV. Georgia kaolin and kaolinizing source rocks. *Clays and Clay Minerals*, **25**, 311–345.

Keller, W.D. (1989) Scanning electron micrographs of clay minerals formed by weathering and other genetic process. Pp. 29–47 in: *Weathering, its Products and Deposits* (K.S. Balasubramaniam *et al.*, editors). Theophrastus Publications, SA., Athens.

Kennedy, V.C. (1964) Sediment transported by Georgia

https://doi.org/10.1346/CCMN.2015.0630401 Published online by Cambridge University Press

streams. U.S.G.S. Water Supply Paper 1668, 54 pp.
Kitagawa, R. and Köster, H.M. (1991) Genesis of the Tirschenreuth kaolin deposit in Germany compared with the Kondachi deposit in Japan. *Clay Minerals*, **26**, 61–79.
Knauth, L.P. (1994) Petrogenesis of chert. Pp. 233–258 in: *Silica: Physical Behavior, Geochemistry and Materials Applications* (P.J. Heaney, C.T. Prewitt, and G.V. Gibbs, editors). Mineralogical Society of America, Washington, D.C.
Koçyiğit, A. and Deveci, Ş. (2007) Çukurören-Çobanlar (Afyon) arasındaki deprem kaynaklarının (Aktif fayların) belirlenmesi. The Project Report of The Scientific and Technical Research Council of Turkey (TÜBİTAK) 106Y209, 71 pp, Turkey (in Turkish).
Konak, N. (2002) Türkiye jeoloji haritası İzmir Paftası. Maden Tetkik Arama Genel Müdürlüğü, 1 p., Ankara (in Turkish).
MacEwan, D.M.C. and Wilson, M.J. (1980) Interlayer and intercalation complexes of clay minerals. Pp. 197–248 in: *Crystal Structures of Clay Minerals and their X-ray Identification* (G.W. Brindley and G. Brown, editors). Monograph **5**, Mineralogical Society, London.
MacLean, W.I. and Kranidiotis, P. (1987) Immobile elements as monitors of mass transfer in hydrothermal alteration: Phelps Dodge massive sulfide deposit, Matagami, Quebec. *Economic Geology*, **82**, 951–962.
Marfil, S.A., Maiza, P.J., Cardellach, E., and Corbella, M. (2005) Origin of kaolin deposits in the Rio Negro Province, Argentine. *Clay Minerals*, **40**, 283–293.
Marfil, S.A., Maiza, P.J., and Montecchiari, N. (2010) Alteration zonation in the Loma Blanca kaolin deposit, Los Menucos, Province of Rio Negro, Argentina. *Clay Minerals*, **45**, 157–169.
Marin-Carbonne, J., Robert, F., and Chaussidon, M. (2014) The silicon and oxygen isotope compositions of Precambrian cherts: A record of oceanic paleo-temperatures? *Precambrian Research*, **247**, 223–234.
Marumo, K., Matsuhisa, Y., and Nagasawa, K. (1982) Hydrogen and oxygen isotopic composition of kaolin minerals in Japan. Pp. 315–320 in: *Siliceous Deposits in the Pacific Region* (A. Iijima, J.R. Hein, and R. Siever, editors). Developments in Sedimentology, **35**, Elsevier, Amsterdam.
Maurice, A.E., Bakhit, B.R., Basta, F.F., and Khiamy, A.A. (2013) Geochemistry of gabbros and granitoids (M- and I-types) from the Nubian Shield of Egypt: Roots of Neoproterozoic intra-oceanic island arc. *Precambrian Research*, **224**, 397–411.
McDonough, W.F. and Sun, S.S. (1995) Composition of the earth. *Chemical Geology*, **120**, 223–253.
Meunier, A. (2005) Isotopic composition of clay minerals. Pp. 153–190 in: *Clays* (A. Meunier, editor). Springer-Verlag, Berlin-Heidelberg.
Miretzky, P., Conzonno, V., and Cirelli, A.F. (2001) Geochemical processes controlling silica concentrations in groundwaters of the Salado River drainage basin, Argentina. *Journal of Geochemical Exploration*, **73**, 155–166.
Montes, C.R., Melfi, A.J., Carvalho, A., Vieira-Coelho, A.C., and Formoso, M.L.L. (2002) Genesis, mineralogy and geochemistry of kaolin deposits of the Jari Rıver, Amapá State, Brazil. *Clays and Clay Minerals*, **50**, 494–503.
MTA (2005) Geothermal resource inventory of Turkey. Series of General Directorate of Mineral Research and Exploration (MTA), No: 201, 739–741, Ankara (in Turkish).
Murray, H.H. (1980) Diagnostic tests for evaluation of kaolin physical properties. *Acta Mineralogica-Petrographica*, **24**, 67–80.
Murray, H.H. (1988) Kaolin minerals: Their genesis and occurrences. Pp. 67–89 in: *Hydrous Phylloslicates* (S.W. Bailey, editor). Reviews in Mineralogy, **19**, Mineralogical Society of America.
Murray, H.H. (2000) Traditional and new applications for kaolin, smectite, and palygroskite: a general overview. *Applied Clay Science*, **17**, 207–221.
Murray, H.H. and Janssen, J. (1984) Oxygen isotopes – indicators of kaolin genesis. *Proceedings of the 27th International Geological Congress*, **15**, 287–303.
Murray, H.H. and Keller, W.D. (1993) Kaolins, kaolins and kaolins. Pp. 1–24 in: *Kaolin Genesis and Utilization* (H.H. Murray, W. Bundy, and C. Harvey, editors). The Clay Minerals Society, Boulder, Colorado, USA.
Nakagawa, M., Santosh, M., Yoshikura, S., Miura, M., Fukuda, T., and Harada, A. (2006) Kaolin deposits at Melthonnakkal and Pallipuram within Trivandrum block, southern India. *Gondwana Research*, **9**, 530–538.
Nichols, G. (2009a) Terrigenous clastic sediments: gravel, sand and mud. Pp. 5–27 in: *Sedimentology and Stratigraphy.* John Wiley and Sons, Ltd., Chichester, UK.
Nichols, G. (2009b) Process of transport and sedimentary structures. Pp. 44–68 in: *Sedimentology and Stratigraphy*, John Wiley and Sons, Ltd., Chichester, UK.
Özyurt, N.N. and Bayarı, C.S. (2005) Isotope applications in the Aladag karstic aquifer, Taurids, Turkey. Symposium of 2nd Isotope Techniques in National Hydrology, İzmir, Turkey.
Patterson, S.H. and Murray, H.H. (1975) Clays. Pp. 519–585 in: *Industrial Minerals and Rocks*, 4th edition (S.J. Lefond, editor). AIME, New York.
Pearce, J.A., Harris, N.B., and Tindle, A.G. (1984) Trace element discrimination diagrams for the tectonic interpretation of granitic rocks. *Journal of Petrology*, **25**, 956–83.
Pevear, D.R., Williams, V.E., and Mustoe, G.E. (1980) Kaolinite, smectite, and K-rectorite in bentonites: Relation to coal rank at Tulameen, British Columbia. *Clays and Clay Minerals*, **28**, 241–254.
Potter, P.E., Maynard, J.B., and Depetris, P.J. (2005) *Mud and Mudstones: Introduction and Overview* (1st edition). Springer, Würzberg, Germany.
Prasad, M.S., Reid, K.J., and Murray, H.H. (1991) Kaolin: processing, properties and applications. *Applied Clay Science*, **6**, 87–119.
Rodgers, K.A., Browne, P.R.L., Buddle, T.F., Cook, K.L., Greatrex, R.A., Hampton, W.A., Herdianita, N.R., Holland, G.R., Lynne, B.Y., Martin, R., Newton, Z., Pastars, D., Sannazarro, K.L., and Teece, C.I.A. (2004) Silica phases in sinters and residues from geothermal fields of New Zealand. *Earth-Science Reviews*, **66**, 1–61.
Ross, C.S. and Hendricks, S.B. (1945) Minerals of the montmorillonite group. U.S. Geological Survey Prof. Paper, **205**, 23–79.
Saleemi, A.A. and Ahmed, Z. (2000) Mineral and chemical composition of Karak mudstone, Kohat Plateau, Pakistan: implications for smectite-illitization and provenance. *Sedimentary Geology*, **130**, 229–247.
Salvi, S. and Williams-Jones, A.E. (1996) The role of hydrothermal processes in concentrating high-field strength elements in the Strange Lake peralkaline complex, north-eastern Canada. *Geochimica et Cosmochimica Acta*, **60**, 1917–1932.
Salvi, S., Fontan, F., Monchoux, P., Williams-Jones, A.E., and Moine, B. (2000) Hydrothermal mobilization of high field strength elements in alkaline igneous systems: evidence from the Tamazeght Complex (Morocco). *Economic Geology*, **95**, 559–576.
Saunders, A.D., Tarney, J., Marsh, N.G., and Wood, D.A. (1980) Ophiolites as ocean crust: a geochemical approach. Pp. 193–204 in: *Ophiolites: Proceedings of the International Ophiolite Symposium, Cyprus, 1979* (A.

Panayiotou, editor). Ministry of Agriculture and Natural Resources, Geological Survey Department, Cyprus.

Savin, S.M. and Epstein, S. (1970) The oxygen and hydrogen isotope geochemistry of clay minerals. *Geochimica et Cosmochimica Acta*, **34**, 25–42.

Savin, S.M. and Lee, S. (1988) Isotopic studies of phyllosilicates. Pp. 189–223 in: *Hydrous Phyllosilicates (Exclusive of Micas)* (S.W. Bailey, editor). Reviews in Mineralogy, **19**, Mineralogical Society of America, Washington, D.C.

Sayın, S.A. (2007) Origin of kaolin deposits: Evidence from the Hisarcık (Emet-Kütahya) deposits, Western Turkey. *Turkish Journal of Earth Science*, **16**, 77–96.

Schroeder, P.A. and Shiflet, J. (2000) Ti-bearing phases in the Huber Formation, an east Georgia kaolin deposit. *Clays and Clay Minerals*, **48**, 151 –158.

Senkayi, A.L., Ming, D.W., Dixon, J.B., and Hossner, L.R. (1987) Kaolinite, opal-CT, and clinoptilolite in altered tuffs interbedded with lignite in the Jackson Group, Texas. *Clays and Clay Minerals*, **35**, 281–290.

Seyhan, I. (1978) Türkiye kaolen yatakları ile hidrotermal cevherleşmeler arasında görülen ilişkiler. *Jeoloji Mühendisliği Dergisi*, **4**, 27–31, Ankara, (in Turkish).

Sheppard, S.M.F. and Gilg, H.A. (1996) Stable isotope geochemistry of clay minerals. *Clay Minerals*, **31**, 1–24.

Sheppard, S.M.F., Nielsen, R.L., and Taylor, H.P. (1969) Oxygen and hydrogen isotope ratios of clay minerals from porphyry copper deposits. *Economic Geology*, **64**, 755–777.

Sheppard, S.M.F. and Gustafson, L.B. (1976) Oxygen and hydrogen isotope ratios of clay minerals from porphyry copper deposits. *Economic Geology*, **71**, 1549–1559.

Siddiqui, M.A. and Ahmed, Z. (2008) Geochemistry of the kaolin deposits of Swat (Pakistan). *Chemie der Erde*, **68**, 207–219.

Sun, S.S. and McDonough, W.F. (1989) Chemical and isotopic systematics of oceanic basalts: implications for mantle composition and processes. Pp. 313–345 in: *Magmatism in the Ocean Basins* (A.D. Saunders and M.J. Norry, editors). Special Publication, **42**, Geological Society, London.

Taşdelen, S. (1987) Banaz (Uşak) Hamamboğazı kaplıcalarının jeolojik ve jeofizik etüdü. MSc thesis, Akdeniz University, 95 pp., Turkey (in Turkish).

Taylor, B.E. (1992) Degassing of H_2O from rhyolite magma during eruption and shallow intrusion, and the isotopic composition of magmatic water in hydrothermal systems. Pp. 190–194 in: *Extended Abstracts, Japan-US Symposium on Magmatic Contributions to Hydrothermal Systems* (J.W. Hedenquist, editor). Geological Survey of Japan Reports, **279**.

Taylor, S.R. and McLennan, S.H. (1985) *The Continental Crust: Its Composition and Evolution*. Blackwell, Oxford, 312 pp.

Temizel, İ. and Arslan, M. (2009) Mineral chemistry and petrochemistry of post-collisional Tertiary mafic to felsic cogenetic volcanics in the Ulubey (Ordu) Area, Eastern Pontides, NE Turkey. *Turkish Journal of Earth Sciences*, **18**, 29–53.

TUIK – Turkey Statistical Institute (2014) *Industry Products Annual Production and Selling Statistics*, 1 p., Ankara (in Turkish).

Weaver, C.E. (1989) Continental transport and deposition. Pp. 189–278 in: *Clays, Muds, and Shales* (C.E. Weaver, editor). Developments in Sedimentology **44**, Elsevier, Amsterdam.

Whitney, D.L. and Evans, B.W. (2010) Abbreviations for names of rock-forming minerals. *American Mineralogist*, **52**, 1649–1661.

Williams, L.A. and Crerar, D.A. (1985) Silica Diagenesis, II. General Mechanisms. *Journal of Sedimentary Petrology*, **55**, 312–321.

Wilson, M.J. (1987) X-ray powder diffraction methods. Pp. 26–98 in: *A Handbook of Determinative Methods in Clay Mineralogy* (M.J. Wilson, editor). Chapman & Hall, London.

Winchester, J.A. and Floyd, P.A. (1977) Geochemical discrimination of different magma series and their differentiation products using immobile elements. *Chemical Geology*, **20**, 325–343.

Yalçın H. and Gümüşer G. (2000) Mineralogical and geochemical characteristics of late Cretaceous bentonite deposits of the Kelkit Valley Region, northern Turkey. *Clay Minerals*, **35**, 807–825.

Yıldız, A. and Dumlupunar, İ. (2009) Mineralogy and geochemical affinities of bentonites from Kapıkaya (Eskişehir, W Turkey). *Clay Minerals*, **44**, 341–360.

Yıldız, A. and Kuşcu, M. (2004) Origin of the Basoren (Kutahya, W Turkey) bentonite deposits. *Clay Minerals*, **39**, 219–231.

Yılmaz, Y., Genç, S.C., Gürer, Ö.F., Bozcu, M., Yılmaz, K., Karacık, Z., Altunkaynak, Ş., and Elmas, A, (2000) When did western Anatolian grabens begin to develop? Pp. 353–384 in: *Tectonics and Magmatism in Turkey and the Surrounding Area* (E. Bozkurt, J.A. Winchester, and J.D.A. Piper, editors). Special Publications, **173**, Geological Society, London.

Yılmaz, Y., Genç, Ş.C., Karacık, Z., and Altunkaynak, Ş. (2001) Two contrasting magmatic associations of northwest Anatolia and their tectonic significance. *Journal of Geodynamics*, **31**, 243–271.

Zielinski, R.A. (1982) The mobility of uranium and other elements during alteration of rhyolite ash to montmorillonite: A case study in the Troublesome Formation, Colorado, U.S.A. *Chemical Geology*, **35**, 185–204.

(*Received 7 April 2014; revised 17 April 2015; Ms. 863; AE: R.J. Pruett*)